Electron-spin relaxation and ordering in smectic and supercooled nematic liquid crystals[a)]

Eva Meirovitch,[b)] Dan Igner, Eva Igner, Giorgio Moro,[c)] and Jack H. Freed

Baker Laboratory of Chemistry, Cornell University, Ithaca, New York 14853
(Received 29 January 1982; accepted 29 June 1982)

We report on careful line shape studies of slow motional and orientation dependent ESR spectra of a deuterated liquid-crystal-like spin probe dissolved in a benzilidene-derivative (40,6) and in cyanobiphenyl derivative (*S*2 and 5*CB*) liquid crystals. The simulation of the ESR spectra is based on the Lanczos algorithm recently applied by Moro and Freed in a general and efficient formulation of slow motional and ordering effects on ESR line shapes. With 40,6 which exhibits monolayer smectic phases, we find that the main change in the spin relaxation upon passing from the nematic to the smectic *A* phase consists of changes occuring in ordering attributable to packing forces on functional groups. Such ordering effects appear to be further enhanced in the S_B phase with consequent alterations in dynamics. With *S*2, which exhibits an interpenetrating bilayer smectic *A* phase, we find unusual ESR spectra in that phase which may be simulated on the basis of a model of cooperative distortions static on the ESR time scale, and superimposed on individual molecular reorientation. This mode is interpreted as a collective chain distortion which affects the orientational distribution of the piperidine ring of the spin probe. A similar phenomenon is observed in the supercooled nematic phase of 5*CB*, which is aligned by an electric field, and evidence is also found that the reorientational dynamics of this ring are affected by interaction with local cooperative modes in the liquid crystal (i.e., a SRLS mechanism previously proposed by Freed and co-workers). Some microscopic characteristics of liquid crystals revealed by this and previous ESR spin probe studies are discussed.

I. INTRODUCTION

Among the various methods used to study liquid crystals, the ESR spin probe technique has proven to be very useful in elucidating dynamic and structural characteristics of these ordered phases.[1-7] In the initial applications of ESR to this field, the emphasis was on the more fluid nematic and smectic phases where molecular motion is rapid and ordering is often relatively low.[1] The major effect on spin relaxation upon passing from the isotropic to the nematic phase is the onset of molecular ordering.[1(a)] The transition from a nematic to a smectic phase is also reflected mainly in changes in ordering characteristics.[1(b)] More subtle effects could also be detected and were interpreted in terms of the individual reorientational mode of the molecular probe being coupled to local collective modes of the surrounding liquid crystalline solvent.[1(b),3(c)] Theoretical models such as the slowly relaxing local structure (SRLS) mechanism,[1(b),2(c),8] fluctuating torques (FT),[1(a),2(c),8,9] and lately a unified theory developed by Stillman and Freed[8] were invoked to interpret the observations. A detailed study of PD-tempone (PDT) in the smectic phases of 40, 6 and 40, 8 (which are benzilidene-derivative smectics built of a rigid benzene-ring core flanked by alkyl chain residues) has shown that as a consequence of changes in the local structure, this probe molecule becomes expelled from the rigid-core region of the smectic layer toward the more fluid chain region.[1(b)] Also, manifestations of the SRLS mechanism were amplified as compared to the nematic phase.[1]

We further extended the ESR study of the smectic phases of 40, 6 and 40, 8 using a larger, rigid, and highly ordered probe, cholestane (CSL).[3(a)] For this probe, molecular reorientation becomes slowed down on the ESR timescale, so complete line shape analysis was required. Again, the results pointed to deviations from a pure reorientational mode of individual probe molecules and were interpreted by assuming that collective local solvent modes are coupled to the reorientational mode (i.e., SRLS). These local modes do not have the properties attributable to the long-range hydrodynamic modes.[1,2(a),2(c)] The hydrodynamic modes are of long enough wavelength that their properties are independent of molecular details, while the local solvent modes directly involve local intermolecular cooperativity.

We have recently investigated the lyotropic liquid crystalline phase $L_\alpha(1)$ of low water content dipalmitoyl phosphatidyl choline (DPPC) bilayers[3(b),3(c)] by similar ESR methods, and we find that the heterogeneity of the bilayer can be mapped out by employing probe molecules varying in size, shape, and conformation, since this leads to substantial differences in their preferred location within the bilayer, their coupling to collective modes, and, in general, their interaction with the solvent liquid crystalline molecules. With probes reporting on the bilayer interface,[3(c)] we detected spectral features which were interpreted in terms of magnetic field effects on the phospholipid headgroups, while with larger probes of a hydrophobic nature[3(b)] we detected unusual spectral patterns which we suggested might be due to cooperative chain distortions.[3(d)]

These studies make clear that if one is to successfully study the detailed dynamic properties of smectic phases, especially the lower temperature and more ordered phases, it is necessary to carefully design the experiments. This includes consideration of the physical, chemical, and structural nature of the liquid crystals themselves as well as the conformational properties

[a)] Supported by NSF Grant No. DMR81-02047.
[b)] Also: Isotope Department, Weizmann Institute of Science, Rehovot, Israel where some of this work was performed.
[c)] Present address: Istituto di Chimica Fisica, Universita di Padova, Padova 35100, Italy.

 0021-9606/82/203915-24$02.10

ACRONYM	NAME	STRUCTURE
40, 6	N—(p—butoxybenzylidene)—p—n—hexylaniline	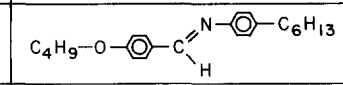
40, 8	N—(p—butoxybenzylidene)—p—n—octylanline	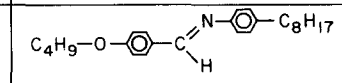
8CB	4—cyano—4′—octylbiphenyl	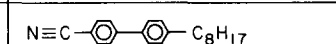
5CB	4—cyano—4′—n—pentyl biphenyl	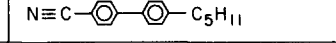
S2	Eutectic mixture of: 4—cyano—4′—n—octyl biphenyl 4—cyano—4′—n—decyl biphenyl 4—cyano—4′—n—decyl oxy biphenyl	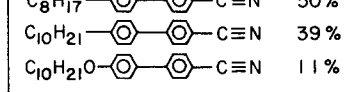
phase Ⅴ	eutectic mixture of four compounds	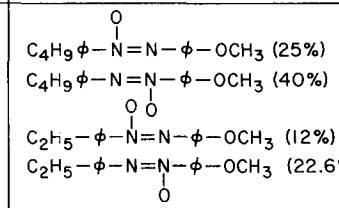
TBBA	terephalylidene—bis—4—n—butylaniline	

FIG. 1. The structures of some liquid crystals and some ESR spin probes discussed in this work.

ACRONYM	NAME	STRUCTURE
P—probe	2—2′—6—6′—tetramethyl 4—(butyl—oxy)—benzoyl—amino piperidine 1—oxyl; (perdeuterated piperidine ring)	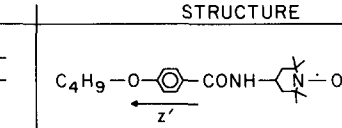
PDT	2,2,6,6—tetramethyl—4—piperidine N—oxide; (perdeuterated)	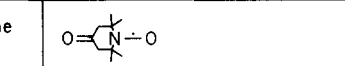
stearamide probe	(4—octadecanoyl) amino—2,2′,6,6′—tetramethyl piperidinyl—1—oxy	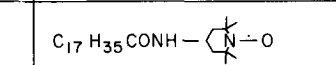
CSL	3′,3′—dimethyloxazolidinyl—N—oxy 2′,3—5α—cholestane	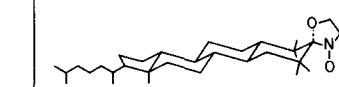
EOTA	4—ethyl amino—2,2,6,6—tetramethylpiperidinyl—1—oxy	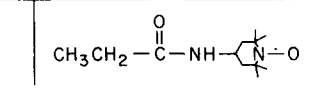

of the probe molecules. In these lower temperature phases, when the structure of the probe molecules resembles that of the liquid crystalline molecules, the ESR spectra typically fall into the slow motional regime. This has two distinct advantages: first, the dynamical behavior of the probe should be a reasonably good approximation to that of the liquid crystal molecules; second, the slow motional regime is the most sensitive to dynamic and ordering effects when properly analyzed.

We have attempted in the present study to optimize such factors. Thus, we have prepared, following Barbarin *et al.*,[10(a)] a relatively large and flexible probe molecule end-labeled by a deuterated piperidine ring bearing the NO group (denoted P in the following) which is similar to typical liquid crystal molecules (cf. Fig. 1). Also, we chose two different types of liquid crystals: viz. 40, 6, which is a benzilidene derivative exhibiting monolayer smectic A and B_A phases between about 50 °C and room temperature; $S2$, an eutectic mixture of cyanobiphenyl derivatives exhibiting a smectic phase between 47 and − 10 °C which is expected to be composed of interpenetrating bilayers, and $5CB$, a pure cyanobiphenyl derivative exhibiting a nematic phase which may be supercooled below 34.3 °C and is readily oriented by electric-field methods (cf. Fig. 1 for their structures).[11]

It is appreciated by many workers that ESR studies of oriented liquid crystals provide considerably more detailed information when studied as a function of orientation of the liquid-crystalline (or nematic) director relative to the magnetic field. The advantages are analogous to those of performing ESR on oriented single crystals. In the smectic phase the director orientation can usually be "frozen-in" so that it does not reorient when the sample is rotated in the magnetic field. In the slow motional regime, however, this necessitates exceedingly complicated computer programs for accurate spectral

simulation for the cases when the director is not parallel to the magnetic field. Successful but cumbersome computer programs written by us[12(a)] and utilized by Meirovitch and Freed[3(b),3(c)] were employed in the study of DPPC bilayers.[3(b),3(c)] A more general formulation, including much greater computational efficiency, has been developed by Moro and Freed,[12(b),12(c)] and it proved to be of great value in the analysis of the experiments reported in the present work.

While the probe P has the advantage of similarity of structure to liquid-crystalline molecules (cf. Fig. 1), it has a potential disadvantage compared to the probes PDT and CSL we have previously employed. That is, there is freedom of the piperidine ring to engage in internal rotations (e.g., about the piperidine C–N bond) relative to the rest of the molecule, and the overall flexibility of the molecule should result in more complex rotational dynamics.[13(a)] To determine the extent to which detailed line shape studies could clarify such processes in liquid crystalline phases is another objective of this work.

We found with P that in the nematic phases of 40, 6 and *S*2 the main features are moderate ordering and anisotropic diffusion. This could imply an important role for the internal motion vs overall molecular reorientation in this ordered fluid. In past work with PDT and CSL, large apparent anisotropy was interpreted in terms of the SRLS mechanism in the absence of any internal rotational modes.

With 40, 6 we found that with the transition to the S_A phase, the ordering of P was no longer axially symmetric, implying that in the smectic phase ordering characteristics are strongly influenced by structural properties of the functional groups as distinct from the overall symmetry of the molecule (which is approximately axially symmetric in shape). This is likely due to constraints imposed on the probe molecule by its restrictive environment. The passage to the S_B phase appears to primarily slow down the (internal) rotation of the piperidine ring along with an increase in the ordering of P.

With the smectic *A* phase of *S*2 we found unique spectral features that are uncharacteristic of smectic *A* molecular alignment. These spectral features are interpreted in terms of first, spin relaxation by molecular reorientation, and second, a cooperative mode, static on the ESR time scale, possibly resulting from cooperative chain distortions, i.e., on the alkyl residues, to which the piperdine ring seems to be strongly coupled. We find that molecular reorientation slows down gradually as the temperature is decreased, while the ordering of the piperidine ring increases substantially.

For purposes of comparison with the behavior of the low-temperature smectics, we have also studied the low-temperature nematic: 5*CB*, which is chemically similar to *S*2. In order to perform angular-dependent measurements on a nematic liquid crystal, one has to apply an electric field E to the sample in order to align the liquid crystalline director *uniquely* independent of the orientation of the magnetic field B; (otherwise the nematic director would "follow" the orientation of B). This technique has been used previously for ESR by Luckhurst and Poupko[13(b)] and others, and we followed their method as described in the experimental section. We found that at higher temperatures in the nematic phase of 5*CB*, spin relaxation is similar to that observed in the nematic phases of 40, 6, *S*2, and in other nematic phases.[1] However, upon supercooling 5*CB*, the ESR spectrum changes in a manner that was unexpected from the higher temperature results to become very similar to that observed in the smectic phase of *S*2, which we interpret in terms of cooperative chain distortions (static on the ESR time scale) that affect the nitroxide moeity at low temperatures even in the nematic phase.

Also, by detailed spectral simulations of the low-temperature 5*CB* results and the related *S*2 results we are able to discern certain spectral anomalies that are strongly reminiscent of those first observed in our earlier study of PD-tempone at low temperatures in the nematic mixture known as phase V (cf. Fig. 1).[1(a)] These line shape anomalies were by an approximate but detailed analysis interpreted as symptomatic of the SRLS mechanism already noted above. We thus conclude that the reorientational *dynamics* of the piperidine ring is also significantly affected by localized cooperative modes of the host molecules in these low temperature liquid crystals.

These various aspects are discussed below in the context of the microscopic characteristics of nematic and smectic phases.

In Sec. II we summarize experimental methods. In Sec. III we describe our experimental results and their analysis, while our conclusions appear in Sec. IV. We give in the Appendices the slow-motional formulation upon which our analyses are based.

II. EXPERIMENTAL

A. Preparation of samples

The spin-probe 2-2′-6-6′-tetramethyl 4-(butyl-oxy)-benzoyl-amino piperidine 1-oxyl was prepared in these laboratories following the procedure of Barbarin *et al.*[10(a)] for a similar nitroxide. The analogous probe, but with the piperidine ring fully perdeuterated, was prepared by Mr. Sidney Wolfe (at UC Berkeley) and kindly supplied to us by Professor Alex Pines. The protonated form was used in preliminary studies, but because of the significantly greater ESR resolution of the perdeuterated form (which we have abbreviated: P), the results reported here are with P.

5*CB* and *S*2 were purchased from BDH Chemicals, Ltd.

40, 6 was prepared by condensing equimolar quantities of 4-*n*-butoxy-benzaldehyde and 4-*n*-hexylaniline in absolute ethanol till a constant melting point was achieved. *S*2 and 5*CB* were used without further purification since the transition temperatures were found to be in good agreement with published values.

It was shown in Ref. 3(a), in a study on 40, 6 that parallel glass plate samples should have the glass sur-

faces specially treated to enhance the homeotropic alignment. Furthermore, the thickness of the liquid crystal sample must not be too great, or else there will be magnetic-field-induced distortions of the director away from perfect alignment relative to the normal to the glass plates when the sample is tilted with this normal at an angle with respect to the magnetic field. Thus, a thickness of 200 μ was found to be satisfactory, while a thickness of 800 μ was completely unsatisfactory for 40,6. Thus, samples of ~200 μ were used for 40,6 in this work. No magnetic-field distortion effects[3(a),3(c)] were detected with the smectic phase of *S*2.

The molecular structures of the spin probe and the various liquid crystals are shown in Fig. 1.

The ESR samples were prepared by addition of P (which is an oily material) to the pure liquid crystals to a final concentration of 5×10^{-4} to 10^{-3} M (the concentrations used were checked to be sufficiently low to avoid concentration-dependent effects on the spectra). The transition temperatures of the pure liquid crystals were found to be lowered by 2°–3° by adding the ESR spin probes. 2 mm i.d. cylindrical tube samples were degassed by the usual freeze–thaw technique on a vacuum line and were sealed off under a vacuum of 10^{-4} Torr. Glass plate samples were prepared and deoxygenated as described previously.[3]

For *S*2, the orientation-dependent ESR spectra obtained with 0.2 mm i.d. cylindrical tube samples were identical to those obtained with glass plates using 200–400 μ spacers. Therefore, about 400 μ spacers, giving a convenient signal to noise ratio, were used. All samples had a geometry appropriate for mounting within the magnetic field using the commerical goniometer of the Varian E-line spectrometers.

B. ESR spectrometer

The ESR measurements were performed on a Varian E-12 spectrometer using 100 kHz field modulation and, whenever necessary, 10 kHz modulation. The temperature in the active region of the cavity was controlled by a Varian E-257 variable temperature control unit to a long term stability of ±0.1 °C. The other aspects of the experimental methods are as described earlier.

C. Aligning the director in the smectic liquid crystalline phases

The sample was first heated to the isotropic or nematic phase, while in the cavity of the E-12 spectrometer and with a 3kG magnetic field present. In the nematic phase the director is aligned parallel to the magnetic field of the spectrometer. The field was increased to 13.5 kG and then the sample temperature was slowly and carefully lowered until the smectic *A* phase was formed. This procedure was cycled a few times near the nematic–smectic *A* phase transition region. For glass-plate samples this procedure was carried out while the normal to the plates was parallel to the external magnetic field.

D. Electric field alignment

The "sandwich geometry" sample cell for the 5*CB* was made from two 3×0.8 cm plates of 0.5 mm thick Nessatron "conducting glass" supplied by PPG Industries, Pittsburgh, Pa., between which a 200 μm mylar spacer was inserted. The cell was glued around with epoxy, except for a small opening. The open cell was submersed under vacuum in degassed, 2×10^{-4} mol probe doped 5*CB*. When N_2 gas was admitted into the vacuum vessel the 5*CB* was sucked into the cell. Subsequently, the opening was epoxy sealed under N_2 atmosphere.

The alignment of the nematic in the cell was achieved by applying to the plates 280 V of 5–15 kHz sinusoidal voltage. Because 5*CB* has both positive dielectric anisotropy and positive conduction anisotropy no electrohydrodynamic instabilities are expected under these conditions,[14(b)] and observations on the electric-field aligned samples with a polarizing microscope showed good homeotropic alignment over the temperature range studied.[14(d)] Possible flexoelectromagnetic instabilities when the sample is under both the electric and magnetic fields are theoretically predicted only for magnetic fields much larger than those used in the present experiment.[14(c)] Such instabilities will be suppressed by the high frequency of the electric field, as will possible flexoelectric instabilities. The ESR spectra obtained with the director aligned parallel to the magnetic field were compared with those obtained from 1 mm i.d. cylindrical tube samples (with no electric fields) and were found to be identical, indicating that there are no significant effects from the conducting glass surfaces[14(d)] nor from the electric fields for this parallel orientation.

III. RESULTS AND DISCUSSION

In our spectral analyses we relied only on complete line shape analysis, based on a visual best fit between experimental and calculated spectra, throughout this study. The results we obtained are summarized in Tables I–IV. For ease in the comparison of parameters for the different probes (utilizing previous studies), between various mesophases of the same liquid crystal,

TABLE I. Magnetic tensors.[a]

	A_x ···	A_y ···	A_z ···	g_x ···	g_y ···	g_z ···	$\langle A\rangle$	$\langle g\rangle$
P in 4,06	6.55	6.7	32.00	2.0094	2.0055	2.0026	15.08	2.0058
P in *S*2	7.4	7.9	31.8	2.0098	2.0062	2.0030	15.70	2.0063
P in 5*CB*	8	8.5	34.3	2.0101	2.0062	2.0027	16.93	2.0063

[a]Hyperfine values are in Gauss.

TABLE II. Ordering parameters and mean correlation times for P in the various phases of 40, 6 at different temperatures.

Temp. (°C)	Mesophase[e]	λ[a,d]	ρ[a]	$\langle D_{00}^2 \rangle$	$\langle D_{02}^2 + D_{0-2} \rangle$	A', G[b]	$\tau_{\langle R \rangle}$[c,d] (s^{-1}) $\times 10^{+11}$	N	E_{act} (kcal/mol)	$R_\parallel \times 10^{-9}$ s^{-1}	$R_\perp \times 10^{-9}$ s^{-1}
100.1	Isotropic	0.0	0.0	0.0	0.0	0.2	7.7			5.73	0.818
72.5		0.0	0.0	0.0	0.0	0.25	20.0	7.0	9.1	5.20	0.315
71.7	Nematic	1.17	0.0	0.26	0.0	0.3	17.4	14.0	7.0	3.58	0.256
50.5		2.00	0.0	0.44	0.0	0.3	34.0			1.83	0.131
49.5	Smectic *A*	2.15	0.0	0.47	0.0	0.4	37.0	10	(4.9)		
		2.5	−0.6	0.52	−0.078	0.4	40.0	20	(5.0)	1.86	0.0932
43.3		2.2	0.0	0.48	0.0	0.5	43.0	10	(4.9)		
		2.9	−0.7	0.58	−0.073	0.5	46.0	20	(5.0)	1.62	0.0810
42.5	Smectic *B*	3.1	0.0	0.62	0.0	0.5	120	3	9.5		
		4.8	−1.7	0.74	−0.069	0.5	125	3	9.9	0.231	0.0720
23.3		3.8	0.0	0.70	0.0	0.5	225	3	9.5		
		5.0	−1.8	0.75	−0.067	0.5	231	3	9.9	0.125	0.0417

[a]The relationship between $\langle D_{00}^2 \rangle$ and λ is given by the following expression:

$$\langle D_{00}^2 \rangle = \int_{\phi'} \int_{\theta'} P(\theta', \phi') \left(\tfrac{1}{2}\right) (3\cos^2\theta' - 1) \sin\theta' d\theta' d\phi'$$

and $\langle D_{02}^2 + D_{0-2}^2 \rangle = \int_{\phi'} \int_{\theta'} P(\theta', \phi') \left(\sqrt{6}/2\right) \sin^2\theta' \cos 2\phi' \sin\theta' d\theta' d\phi'$, where θ' denotes the angle between the principal axis z' of the ordering tensor and the principal axis z'' of the director frame. $P(\theta', \phi') \sin\theta' d\theta' d\phi'$ is the distribution of z' relative to z'' given by $P(\theta', \phi') \propto \exp[-\lambda \tfrac{1}{2}(3\cos^2\theta' - 1) + (\sqrt{6}/2)\rho \sin^2\theta' \cos 2\phi']$.

[b]A' denotes the intrinsic linewidth in Gauss.

[c]$\tau_{\langle R \rangle} \equiv 6^{-1} (R_\parallel R_\perp)^{-1/2}$ and $N = R_\parallel / R_\perp$.

[d]The accuracy in the values of τ_R and λ was estimated to be about 8%.

[e]Transition temperatures of spin probe doped 40, 6.

40,6: Sm B_A	Sm *A*	Nematic	Isotropic
	42.8°	49.9°	72.1°

and between different liquid crystals, we have included in these tables only values related to extreme temperatures in each mesophase, while the detailed temperature dependences of the motional rates are illustrated graphically in Fig. 2.

The magnetic parameters for P in the various liquid crystals were determined by complete line shape simulation of the experimental rigid limit spectra obtained at −150 °C. These results are listed in Table I for the different solvents. A surprising result is the significantly different magnetic parameters obtained for P in 5*CB* compared to P in *S*2 despite the chemical similarities of the two solvents. This matter is discussed below (cf. Sec. III D).

In our discussion below we introduce several reference frames: (1) the laboratory frame (specified by Cartesian coordinates x, y, z) in which the z axis is parallel to $\mathbf{B}_0$; (2) the director frame (x'', y'', z'') in which the z'' axis is parallel to the nematic director; (3) the molecular diffusion frame (x', y', z') constituting the principal axes of the molecular rotational diffusion tensor; and it will be assumed that these are also the principal axes for

TABLE III. Ordering parameters and mean correlation times for P in *S*2.

Temp (°C)	Mesophase[a]	λ	ρ	$\langle D_{00}^2 \rangle$	$\langle D_{02}^2 + D_{0-2}^2 \rangle$	A', G	$\tau_{\langle R \rangle}$ (s^{-1}) $\times 10^{+10}$	N	E_{act} (kcal/mol)
100.1	Isotropic	0.0	0.0	0.0	0.0	0.2	1.1	6	12.0
47		0.0	0.0	0.0	0.0	0.25	11.0		
46	Nematic	0.97	0.0	0.21	0.0	0.4	13.5	(6)	...
44.5	Smectic *A*	1.0	−0.5	0.21	−0.14	0.5	17.0	4	1.5
−9		6.0	−0.8	0.82	−0.018	0.8	32.0		

[a]Transition temperatures of spin probe doped *S*2:

*S*2: Solid	Sm *A*	Nematic	Isotropic
	−11.0°	45.5°	46.5°

TABLE IV. Ordering parameters and mean correlation times for P in 5*CB*.

Temp (°C)	Mesophase[a]	λ	ρ	$\langle D^2_{00}\rangle$	$\langle D^2_{02}+D^2_{0-2}\rangle$	A', G	$\tau_{(\bar{R})}$ (s^{-1}) $\times 10^{+10}$	N	E_{act} (kcal/mol)
54.5	Isotropic	0.0	0.0	0.0	0.0	0.22	3.8	10	10.7
35.6		0.0	0.0	0.0	0.0	0.28	8.9		
28	Nematic	0.82	0.0	0.18	0.0	0.4	10.1	10	~(10.0)
25		1.5	0.0	0.33	0.0	0.5	14.2		
18.0		1.8	0.0	0.4	0.0	1.0	17.4	4	~(4.0)
3.0		2.5	0.0	0.53	0.0	1.2	20.0		

[a]Transition temperatures of spin probe doped 5*CB*:

5*CB*: Solid | Nematic | Isotropic

→ 25° 35.6°

← supercooling

the molecular ordering tensor with respect to the nematic director; (4) the molecular magnetic tensor frame (x''', y''', z''') in which the $\tilde{g}$ and $\tilde{A}$ tensors are diagonal.

A. P in 40,6

We found that in the isotropic phase the mean correlation time $\tau_{\bar{R}}$ defined as $(1/6)\,(R_{\parallel}\cdot R_{\perp})^{-1/2}$ [with $R_{\parallel}$ and $R_{\perp}$, respectively, denoting the motional rates (in units of s^{-1}) parallel and perpendicular to the principal axis z' of the diffusion tensor] increases from 7.6×10^{-11} s at 100 °C to 2×10^{-10} s at 72.5 °C, corresponding to the motional narrowing region. We find that z' is parallel to the magnetic x''' axis (cf. Fig. 1), as expected for an extended conformation of the probe molecule, where the long molecular axis is approximately

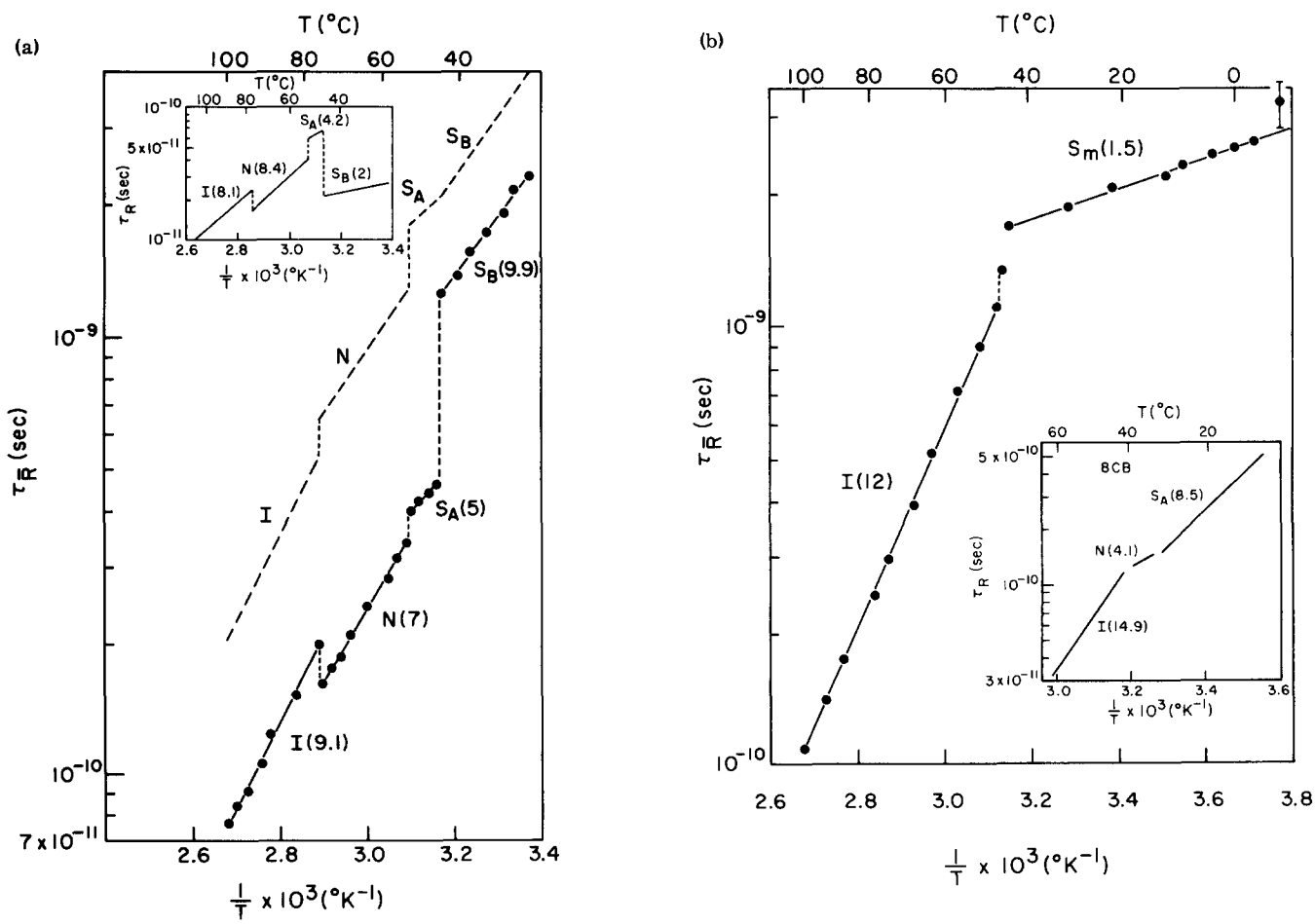

FIG. 2. $\tau_{\bar{R}}$ vs $1/T$ for the P probe in (a) 40.6 and (b) S2 shown with the experimental points. The dashed lines in (a) show $\tau_{R_\perp}$ vs $1/T$. The inserts are reproduced from Fig. 11, Ref. 1(b).

parallel to the N–O bond, and therefore to the magnetic x''' axis. The anisotropy parameter N (defined as $N = R_{\parallel}/R_{\perp}$) was found to be approximately 7, which is consistent with an elongated shape[10,15] and with some internal rotation of the piperidine ring relative to the rest of the chain. More precisely, we estimate an N of about 4 for a hydrodynamic prolate ellipsoid[15] with the long axis dimension of $r_{x'''} \approx 10$ Å corresponding to half the length of the fully extended molecule and the short axes with dimensions of $r_{y'''} \approx r_{z'''} \approx 2.85$ Å for the piperidine ring. Thus, it is likely that some internal rotation of the piperidine ring is also occurring.[13(a)] [It is interesting to note that an $N \approx 3$–3.5 was found by Barbarin *et al.*[10(b)] for the longer $C_8H_{17}O$ analog of P in simple solvents, in which the conformation is presumably not elongated]. The detailed temperature dependence of $\tau_{\bar{R}}$ is illustrated graphically in Fig. 2 and corresponds to an activation energy of 9.1 ± 0.2 kcal/mol. (The uncertainty shown here and below is actually the precision.)

In the nematic phase, the ordering could be fit with an axial ordering about x''', with the dimensionless orienting potential $\lambda_{x'''}$ increasing from 1.17 at 71.7 °C, to 2.0 at 50.5 °C as shown in Table II.[16] While $\tau_{\bar{R}}$ is observed to decrease by about 10% upon passing from the $I-N$ phase, there appears to be an increase in N to about 14, which would imply that $R_{\perp}$ has decreased by almost 20%, while $R_{\parallel}$ has *increased* by more than 50% (see below). The value of E_a is found to be 7.0 ± 0.2 kcal/mol. [We did not attempt to reanalyze these results with a nonaxial ordering model (see below) in view of the good fit and the availability of only the $\theta = 0°$ spectrum.]

We now discuss the analysis of the ESR spectra of P in the smectic A and B_A phases of 40,6.

In Fig. 3 we present temperature and angular dependent ESR spectra and our attempts to fit these by using the values of N, $R_{\perp}$, and λ obtained in the nematic phase as initial guides.[16] The best-fit calculated spectra obtained by varying λ and $R_{\perp}$ are shown by the dashed lines in Fig. 3; obviously, this is a rather poor fit. We then tested three models, each of which implies some qualitative change in the properties of P in the smectic phases. In model 1 we allowed for a nonzero tilt angle between the principal diffusion (and ordering) axis z' and the principal magnetic axis x'''. This would imply a smectic-phase-induced tilting of the piperidine moiety containing the N–O bond, relative to the primary, or fast, axis of rotation. This axis need not necessarily be the long molecular axis especially if there is internal rotation and local ordering of the piperidine moiety. We could *not* improve the fit with this model. Next we tried model 2, wherein we replaced the one-term (dimensionless) orienting potential $U/kT = -\frac{3}{2}\lambda \cos^2\beta$ (where $\Omega = \alpha, \beta, \gamma$ represents the Euler angles between molecular axes x', y', z' and the lab frame defined by the main director) by a two term potential of form $-\lambda_0^2 D^2_{0,0}(0,\beta,0) - \lambda_0^4 D^4_{00}(0,\beta,0)$ (which may be rewritten in the form $-a\cos^2\beta - b\cos^4\beta$) and which still preserves cylindircal symmetry but allows for a more complex variation of the potential with respect to angle β [cf. Ref. 2(b) and Appendix], a model popular with other workers.[4–7,10]

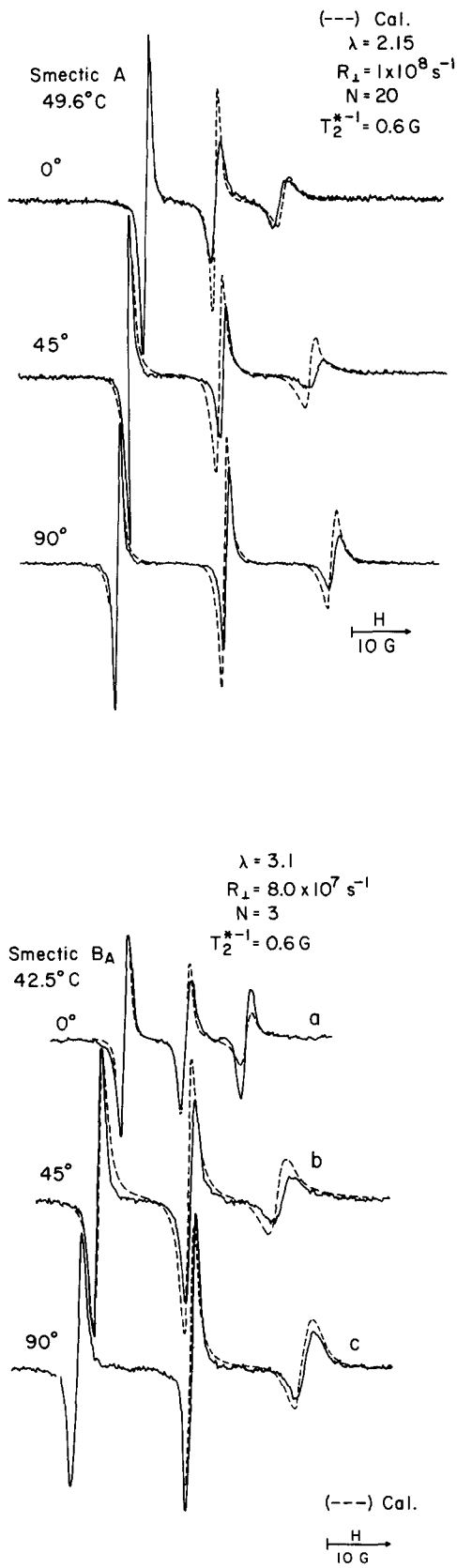

FIG. 3. (–) Experimental ESR spectra of 10^{-3} M P probe dissolved in 40,6 in a 150 ± 50 μm thick plate sample in the smectic A and B_A phases of 40,6 at 49.5 and 42.5 °C, respectively, with θ, the angle between B and the plate normal n_m as denoted in the figure; (- - -) calculated spectra with $\lambda = 2.15$, $R_{\perp} = 1 \times 10^8$ s^{-1}, $N = 20$, and $T_2^{*-1} = 0.6$ G for smectic A and $\lambda = 3.1$, $R = 1.4 \times 10^7$ s^{-1}, $N = 4$, and $T_2^{*-1} = 0.6$ G for smectic B_A.

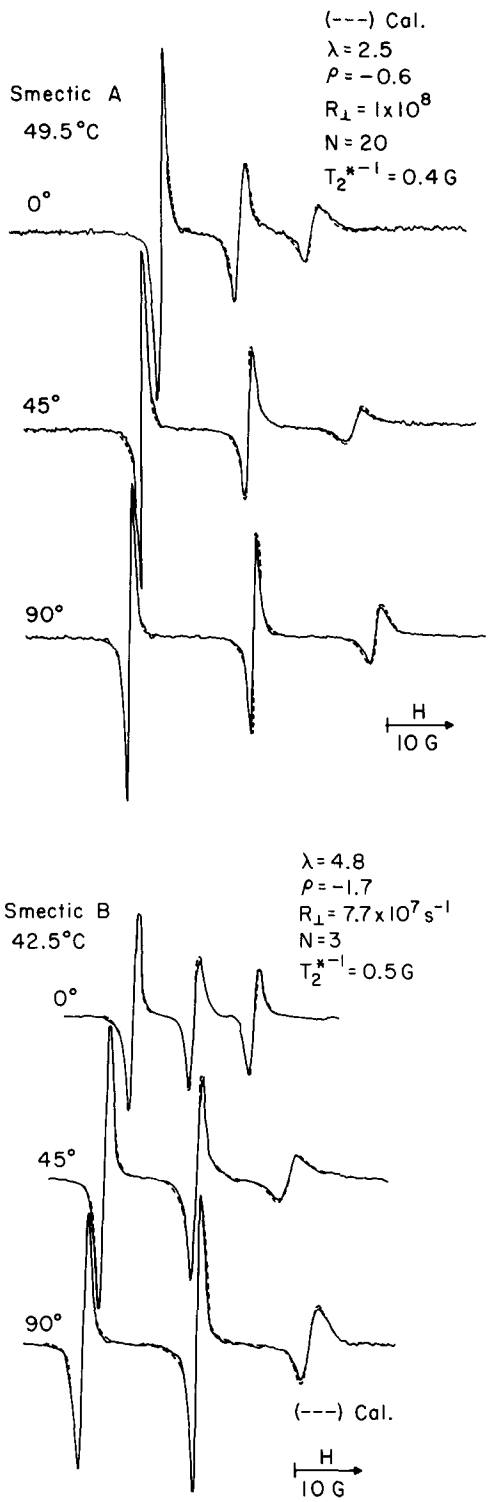

FIG. 4. (–) same as in Fig. 3; (- - -) calculated spectra with $\lambda = 2.5$, $\rho = -0.6$, $R_\perp = 9.3\times10^7\ s^{-1}$, $N = 20$, and $T_2^{*-1} = 0.4$ G for smectic A; and $\lambda = 4.8$, $\rho = -1.7$, $R_\perp = 7.6\times10^7\ s^{-1}$, $N = 20$, and $T_2^{*-1} = 0.5$ G for smectic B_A.

With this model we could improve the relative intensities of the three hyperfine components, but the relative splitting between the $m = -1$ and $m = 0$ hyperfine lines vs that between the $m = 0$ and $m = +1$ hyperfine lines was still unsatisfactory. In model 3 we allowed for deviations from a cylindrically symmetric orienting potential by adding to $-\frac{3}{2}\lambda\cos^2\beta$ the dimensionless asymmetry term: $-(\sqrt{6}/2)\rho\sin^2\beta\cos 2\alpha$, which we have found useful for other probes in the past (cf. Ref. 1 and Appendix A).[16] We obtained our best fit with this model as illustrated in Fig. 4. (In view of the fit, we did not try any combinations of models 1, 2 and 3 plus readjustments of the other parameters.) In general, we have found that the relative splittings between the hyperfine lines is very sensitive to the symmetry of the ordering tensor, even for fast motional spectra, so this criterion was used extensively in our fits.

This asymmetric term implies that while the primary molecular ordering is with respect to the $z' = x'''$ axis, at least for the piperidine moiety of P, there is some preferential ordering of the $z''' = y'$ vs $y''' = x'$ axes perpendicular to the nematic director [e.g., from Table I of Ref. 1(a) we find: $\langle D^2_{00}\rangle_{z'=x'''} = 0.53$, $\langle D^2_{00}\rangle_{y'=z'''} = -0.31$, and $\langle D^2_{00}\rangle_{x'=y'''} = -0.21$ at 49.5 °C, while at 24° these values are 0.75, −0.42, and −0.33, respectively]. One cannot say just from our result to what extent this preferential ordering exists in the functional groups of P other than the piperidine ring. It is not unreasonable to expect that in the smectic A phase (as compared to the nematic phase) with increased packing of the liquid crystal molecules,[17] structural properties of the functional groups can influence the details of their ordering, as suggested by previous results with PD-tempone in 40, 6 and other liquid crystals.[1(a)] To the extent that model 1 is inconsistent with the experimental results (but recall we did not try this model in conjunction with the others), there is no significant change in the primary diffusion (and ordering) axes characterizing the piperidine group in particular (and possibly P as well). On the other hand, our best simulations are consistent with some increase in both $\tau_{\bar{R}}$ and N as one passes from $N - S_A$. The increase in these parameters is equivalent to (cf. Table II) no change in $R_\parallel$ but a decrease in $R_\perp$ (or else it could be indicative of contributions from the SRLS or FT mechanisms as discussed previously for other probes[1,3(a)]). Thus, the internal rotational dynamics of the piperidine ring would appear to be largely unaffected, although the greater packing forces on the whole molecule are leading to greater frictional forces against overall reorientation. Also there appears to be a further small decrease in E_a to 5 kcal/mol, but the small temperature range of the S_A phase makes this value uncertain.

The changes in spin relaxation in crossing the $S_A - S_B$ transition are more dramatic [cf. Fig. 2(a) and Table II]. That is, $\tau_{\bar{R}}$ is found to increase nearly threefold, while N appears to decrease substantially to about 3, and E_a in the S_B phase doubles as compared to the S_A phase. This implies that $R_\perp$ remains at about $8\times10^7\ s^{-1}$ in crossing the $S_A - S_B$ transition, but $R_\parallel$ decreases dramatically from 1.6×10^9 to $2.3\times10^8\ s^{-1}$. This probably implies increased frictional forces on the piperidine moiety, thus slowing down its internal rotation, a feature consistent with the increased molecular packing of the aromatic functional groups within the smectic layer (with a characteristic hexagonal unit cell[17]).

It is useful at this point to compare the temperature dependences of $\tau_{\bar{R}}$ for P in 40, 6 with PDT in this solvent,

so we have added the appropriate insert into Fig. 2 from Ref. 1(a). [Actually, because of the motional narrowing analysis used by Lin and Freed for PDT, the graph shows $\tau_{R(B)}$ which is closely related to $R_\perp$ but with the primary rotation axis taken as y'''.[1(b)] Thus, we have also shown $\tau_{R_\perp} \equiv (6R_\perp)^{-1}$ for P in 40, 6 in Fig. 2(a) for comparison.] We find many close similarities between $\tau_{R_\perp}$ for P vs τ_R for PDT over the range of the I, N, and S_A phases including the small discontinuities at the phase transitions even though the former is about 20–40 times slower than the latter consistent with the greatly increased size of P vs PDT (when the former is in a fully extended configuration). There is even a close similarity (within the uncertainties of the detailed analyses) of the E_a and their variation with phase, except for the S_B phase. These similarities are particularly obvious for the I and N phases. However, the significant drop in $\tau_{R(B)}$ for PDT in passing from the $I \rightarrow N$ phase correlates better with a comparable drop in $\tau_{R_\parallel} \equiv 1/6R_\parallel$ for P than with its increase in $\tau_{R_\perp}$ [cf. Table II and Fig. 2(a)]. We have already implied that this drop in $\tau_{R_\parallel}$ may be due to internal rotational effects of the piperidine ring. Thus, the correlation of $\tau_{R_\parallel}$ with τ_R for PDT (which is basically just the piperidine ring) seems sensible. In the case of the $N \rightarrow S_A$ transition, it is $\tau_{R_\perp}$ which increases for P. But in this case we expect different dynamic behavior for P vs PDT.

The significant decrease in E_a for PDT in the S_A phase was interpreted in terms of this small probe becoming expelled in the lower temperature phase from the rigid core region of the smectic layer (due to increased packing) toward the more fluid alkyl chain region.[1(b)] It may be that P is experiencing greater dynamic interactions with the alkyl chain regions of the liquid crystal in passing from $I \rightarrow N \rightarrow S_A$. This would be consistent with what appears to be a gradual reduction in its E_a. However, the ordering potential terms λ and ρ do increase with decreasing T as expected for increased ordering, unlike the unusual behavior of PDT such that both λ and ρ decrease in magnitude upon lowering T in the S_A phase. Thus, for this reason, as well as for geometrical considerations, it is not to be expected that P can actually be "expelled" from the rigid core region of the liquid crystal, even though interaction with the alkyl chains may well be playing an increased role in its dynamics.

There is, however, a pronounced difference in behavior between P vs PDT in passing from $S_A \rightarrow S_B$, which is now believed to be a strongly first order transition (at least for the similar liquid crystal 40, 8[18]). In the S_B phase the smectic layered structure is more frozen in to yield the hexagonal close packed structure with strong interlayer correlations leading to three dimensional positional ordering,[18] although (cooperative) dynamical reorientation of the individual molecules is expected. The dramatic decrease in τ_R for PDT in the S_B phase, evidence for the large increase in SRLS, and the very low E_a was interpreted by Lin and Freed as due to a slowing down of the hydrocarbon end chains such that PDT is in a fairly well-defined cavity with reduced friction, but the residual end-chain motions effectively modulate the structure of the cavity leading to a significant SRLS mechanism.[1(b)] The long probe P is clearly affected differently by the increased structural order and partial freezing out of motions. It is most likely trapped in the smectic layer, so that its E_a is largely determined by dynamic interaction with the rigid core structure, and less by the hydrocarbon chain. This also significantly enhances the ordering of P. The lack of change of $R_\perp$ at the $S_A \rightarrow S_B$ transition, however, implies no change in the microscopic friction associated with the reorientation of the long axes of P (and most likely the liquid crystal molecules) even while the average ordering is increased,[19] while, as suggested above, the increased packing forces on functional groups may well be reducing internal motion of the piperidine ring.

B. P in the isotropic and liquid crystalline phases of *S*2

In the isotropic phase of liquid crystal *S*2 we find $\tau_{\bar{R}}$ increasing from 1.1×10^{-10} s at 100 °C to 1.1×10^{-9} s at 47 °C, anisotropic diffusion about x''' with $N \simeq 6.0$ and a (high) E_a of 12 kcal/mol. In the nematic phase near the $I \rightarrow N$ transition, $\tau_{\bar{R}}$ increases to 1.35×10^{-9} s, and the spectrum could be satisfactorily simulated with $N = 6$. Due to the very narrow temperature range of the nematic phase (only about 1 °C), no detailed analysis of the spin relaxation in this mesophase was possible. In the smectic phase near the $N \rightarrow S_A$ transition, $\tau_{\bar{R}}$ assumes a value of 1.7×10^{-9} s at 44.5 °C, which increases to approximately 3×10^{-9} s, at −9 °C, the lower limit of the smectic phase. The activation energy was found to be very low, about 1.5 kcal/mol. The detailed temperature dependence of $\tau_{\bar{R}}$ in the various phases is illustrated in Fig. 2(b). The ordering was found to be asymmetric and temperature dependent in the S_A phase with $\lambda = 1.0$ and $\rho = -0.5$ at 44.5 °C and $\lambda = 6.0$ and $\rho = -0.8$ at −9 °C. The value of $N = 4$ is a little reduced from that for the isotropic phase. We note that the results for the smectic phase of *S*2 were obtained by a spectral analysis implying a different model from that considered so far, a matter that will be discussed in detail in Sec. C.

It is again instructive to compare the results obtained with P in *S*2 with those obtained with PDT in a similar (but not identical) solvent 8*CB*.[1(b)] Both solvents are of the cyanobiphenyl type (cf. Fig. 1). The results for PDT in 8*CB* taken from Lin and Freed are shown as an insert to Fig. 2(b). Again, for comparable temperatures in the isotropic phase, the τ_R for PDT are about an order of magnitude shorter than $\tau_{R_\perp}$ [recall $\tau_{\bar{R}}$ is plotted in Fig. 2(b)], but the E_a are both large and comparable. However, in the S_A phase, the low E_a of 1.5 kcal/mol for P in *S*2 is *not* consistent with the substantial value of 8.5 kcal/mol for PDT in 8*CB*. Another unusual feature is the rather low ordering of P in *S*2 at the higher T end of the S_A phase; in magnitude (but not in preferred direction or asymmetry) it is comparable to that of PDT in 8*CB* in the S_A phase (for which $\langle D^2_{00}\rangle_y \sim 0.15$) and substantially less than for P in 40, 6 (cf. Table II). We would take these observations as likely implying a location for P in the S_A phase of *S*2 such that its motional dynamics *and* ordering are strongly affected by the hydrocarbon chain region and this region is becoming increasingly ordered with decreasing T. The reduction in observed N could be implying increased

packing and frictional forces on the functional groups such as the piperidine ring.

Further discussion rests upon our analysis required to explain the unusual features seen in the spectra of Fig. 5(a) for P in the S_A phase of $S2$.

C. P in the smectic phase of $S2$: Cooperative chain distortions

We now wish to discuss the unusual spectral features shown in Fig. 5(a) for P in the S_A phase of $S2$. These unusual features, in which the ESR spectrum becomes spread over a wide range in magnetic field and additional peaks appear, are much different from those exhibited by P in the S_A and S_B phases of 40, 6 (cf. Figs. 3 and 4), which are characteristic of nitroxide probes dissolved in a well-aligned and uniaxial medium with a single well-defined director. The possibilities one may consider to attempt to explain these features are (1) changes in the macroscopic alignment (or texture) of the sample leading to a distribution of directors; (2) microscopic changes, possibly molecular in nature, leading to a distribution of directors; or (3) slow motional effects; or some combination of (1)–(3).

We first discuss possible changes in macroscopic alignment to show that it is not a viable explanation. First of all, the spectra we obtain for P in the nematic phase of $S2$ and in *all* liquid crystalline phases of 40, 6 are consistent with well-aligned homeotropic plate samples. These plate samples, especially including P in the S_A phase of $S2$, were carefully examined under the polarizing microscope. Their optical properties in parallel light between crossed polarizers were found to behave like isotropic liquids as expected for uniform homeotropic alignment with the uniaxial director n normal to the glass plates. Magnetic fields can induce distortions of the alignment if the thickness of the samples is too great [cf. Sec. II and Ref. 3(a)], but we restricted our samples to ~400 μ thickness and checked our results with tube samples of 0.2 mm i.d., (cf. Sec. II). Furthermore, the unusual spectral features are most prominent when $\theta = 0°$ corresponding to $\mathbf{n} \parallel \mathbf{B}$ for which no distortions of the ordering are predicted or observed even with thick plate samples or tubes [cf. Refs. 1(b) and 3(a)]. [The angle θ is, more generally, the angle between n and B.]

We believe that strong evidence against possibility (1) is offered by ESR experiments in which PDT and CSL were used as probes of the S_A phase of $S2$.[20(a)] For both cases, (i.e., the small weakly ordered probe PDT with $\langle D^2_{00}\rangle \approx 0.1$ and the large and highly ordered CSL probe with $\langle D^2_{00}\rangle \approx 0.6$), one obtains orientation-dependent spectra consistent with a well-aligned and uniaxial S_A phase (cf. Fig. 5(c) for CSL in $S2$). These observations suggest that both PDT and CSL are located within (or largely ordered by) the rigid-core region of the smectic layer, while P is mainly affected by the alkyl-chain region as we inferred in the previous section. (We recall that for PDT in 8CB, the analysis[1(b)] suggested that this probe is close to the rigid core region of this cyanobiphenyl liquid crystal in the S_A phase.[20(b)]) On the other hand, spectra quite similar to those obtained with P were also obtained with a stearamide probe (cf. Fig. 1) and with shorter homologs of the latter (e.g., EOTA, cf. Fig. 1).[20(a)] These differences with different probes strongly suggest that the unusual spectral features are related to microscopic features, molecular in detail and probably due to possibility (2) above.

We now show that slow motional effects (3) *alone* are insufficient to explain our results. At the highest temperatures in the S_A phase (e.g., 44.5 °C) no unusual features are obvious in the spectrum, and this can be analyzed in detail to show rather weak ordering ($\lambda = 1.0$, $\rho = -0.05$) and substantial motion with $\tau_{\bar{R}} = 1.7 \times 10^{-9}$ s and $N = 4$ [cf. Fig. 5(b) and Table III]. If we now assume, as is usual, that the motion slows down considerably, and the ordering increases substantially, we would get spectra of the type illustrated in Fig. 6 for $\theta = 0°$. These, and other spectra we have simulated, are completely inconsistent with the lower temperature S_A spectra given in Fig. 5(a). We are thus left with consideration of effects of possibility (2).

The spectra of Fig. 5(a), in particular their unusual features, bear a close similarity to spectra previously reported for nitroxide-labeled phospholipids, fatty acids, and CSL in the lamellar $L_\alpha(1)$ phase of a low water content lyotropic, viz. the lipid DPPC,[3(b)] that in many respects is similar to an S_A phase. [It was also found that spectra of CSL in the low temperature smectic B_C (also called H) phase of the thermotropic liquid crystal TBBA (cf. Fig. 1) exhibited very similar features to those reported for CSL in the $L_\alpha(1)$ phase of DPPC.[3(b)]] The explanation suggested for these spectra was in terms of molecular features leading to microscopic distributions of the local director associated with the chains.[3(d)] It seems reasonable, to attempt a similar explanation for the spectra in Fig. 5(a).

We first briefly review the model of the cooperative distortion mode of the chains. The basic features are (i) the probes showing these effects are located within the hydrocarbon chain region of the oriented bilayer; (ii) there are chain distortions, so that we must define a "local" chain-director $\hat{n}^c_i(\mathbf{r})$, which depends upon the location of the chain specified by $\mathbf{r}$, and that is not, in general, parallel to the mean chain director $\hat{d}_c$ [which is (almost) normal to the aligning plates, i.e., parallel to z'']; (iii) in each region of the sample $\hat{n}^c_i(\mathbf{r})$ is of the form of a coherent wave with component $n^c_{i,z'} = \cos\theta'$ along z'', and components $n^c_{i,x'} = \sin\theta' \cos\phi'$ and $n^c_{i,y'} = \sin\theta' \sin\phi'$ in the x''–y'' plane (i.e., parallel to the aligning plates); where $\theta'(\mathbf{r}) = (2\pi/p) y^c_i(\mathbf{r})$ with p the pitch or wavelength of the wave along the y'_i axis which lies in the x''–y'' plane; (iv) the $y^c_i(\mathbf{r})$ axis is randomly distributed in different regions of the sample (the extent of these regions, i.e., the coherence length is not known except in terms of the spectral constant noted below), so that ϕ' (the angle between y^c_i and y'') is randomly distributed over the sample; (v) this corresponds to a distribution function in θ' and ϕ': $P(\theta', \phi') \propto 1/\sin\theta'$ over the whole sample, where θ' and ϕ' denote the polar and aximuthal angles of the local director in the mean director frame[21(a)]; (vi) the probe molecule at $\mathbf{r}$ experiences mean orienting forces relative to the local director $\hat{n}^c_i(\mathbf{r})$

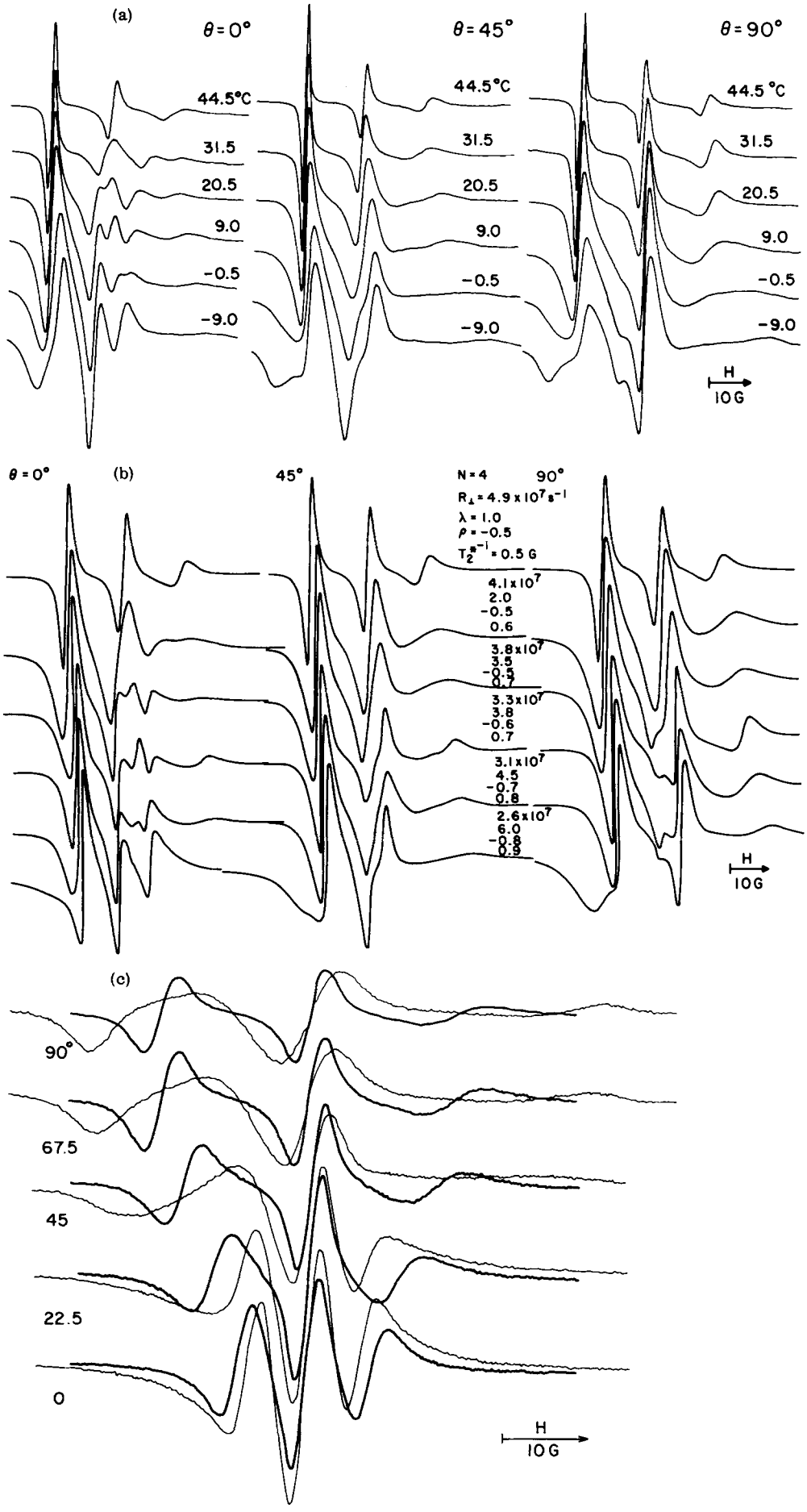

FIG. 5. (a) Experimental ESR spectra of 10^{-3} M P probe in the smectic A phase of $S2$ in a 400 ± 50 μm thick plate sample at temperatures as denoted in the figure for various orientations θ between $\hat{n}_m$ and **B**. (b) Calculated ESR spectra with $N = 4$ and λ, ρ; $R_\perp$ and T_2^{*-1} as denoted in the figure and the distribution function $P(\theta', \phi'') = (\sin\theta')^{-1}$, with θ' denoting the angle between the ordering axis z'' and $\hat{n}_m$. Details on these calculations are given in the text. (c) Experimental ESR spectra of 5×10^{-4}M CSL in the smectic A phase of $S2$ at 25 °C. (dark lines) and -8 °C (light lines) for various orientations θ as denoted in the figure.

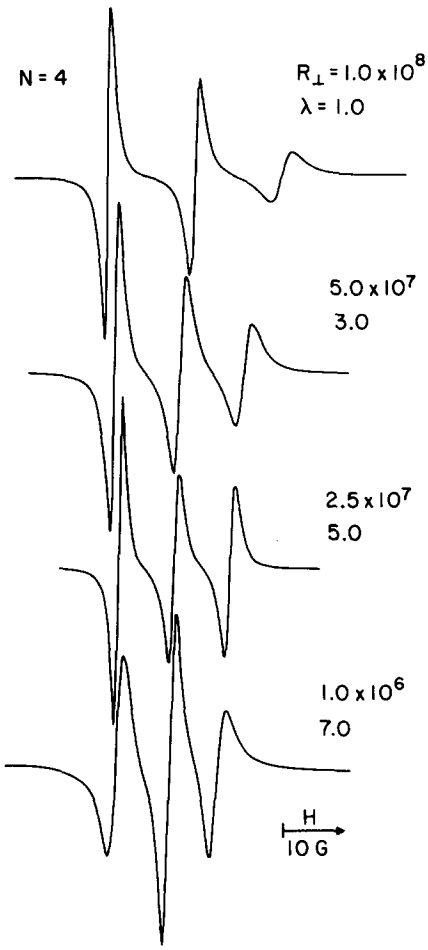

FIG. 6. Calculated ESR spectra with λ, $R_\perp$, N as denoted in the figure, and uniaxial ordering.

as it dynamically reorients and translates, and its translational motion is slow enough that the static distribution of $\hat{n}_i^c(\mathbf{r})$ is manifest in the ESR spectrum. (This last condition requires that $p^2 \gg 24\pi^2 D_T \times (10^{-9}\ \text{s})/\langle D_{00}^2 \rangle$, where D_T is the translational diffusion coefficient[3(b),21(b)].) These coherent modes representing the chain distortions are thus oscillations in the $z''-y_i^c(\mathbf{r})$ plane yielding the character of an isotropic two-dimensional distribution. Physically, it implies substantial cooperativity in chain bends, kinks, etc. between chains of adjacent liquid crystalline (or lipid) molecules in the ordered phases with substantial packing effects on the molecules (i.e., the coherent length as well as the pitch is great enough that the translational motion of the probe does not average it out). It was also shown[3(b)] that by careful simulation of well-resolved spectra, one could distinguish the spectral effects of this $2D$ distribution $P(\theta', \phi')$ from other distributions characteristic of considerable randomness or mosaicity in the sample alignment (cf. also Sec. D).[21(c)]

Actually, the spectral simulations are based upon computing different spectra as a function of the angle $\psi \equiv \cos^{-1}[\hat{n}_i^c(\mathbf{r}) \cdot \hat{b}] = \psi(\theta, \theta', \phi')$ (where $\hat{b} \equiv \mathbf{B}/|B|$ and is the unit vector parallel to the lab z axis)[1,3(b)]; more precisely $\cos\psi = \cos\theta\cos\theta' - \sin\theta\sin\theta'\cos\phi'$. We first let $P(\theta', \phi')\sin\theta'\, d\theta'\, d\phi' = d\theta'\, d\phi'$ and recognize that the ESR spectra depend only on ψ (and not on ϕ'). Thus, one first calculates spectra for different values of ψ ranging from 0° to 90° to yield $I(B, \psi)$. Then the composite spectrum $I(B, \theta)$ is calculated by numerically performing the integral over θ' and ϕ' utilizing the $I[B, \psi(\theta, \theta', \phi')]$ where the correct ψ for a given set of θ, θ', and ϕ' is determined from the cosine law given above.

In practice we solve the eigenvalues and eigenvectors, which determine the spectrum[12] for ten equally spaced values of ψ between 0° and 90°, and then we interpolate them to yield sets of eigenvalues and eigenvectors for 40 values of ψ. This is sufficient for convergence. These values are stored and called as needed for the numerical integration.

Line shapes were then calculated for different values of θ and compared to the experimental spectra.

We used the distribution function $P(\theta', \phi') = (\sin\theta')^{-1}$, and the best fit between calculated and experimental spectra was obtained with values of λ, ρ, $R_\perp$, N, and T_2^{*-1} shown in Fig. 5(b).[22(a)] (Note that the high temperature spectrum at 44.5 °C could equally well be fit with a $1/\sin\theta'$ distribution and with the simple uniaxial model, but the lower temperature spectra all require the $1/\sin\theta'$ distribution.) It is clear from a comparison of Figs. 5(a) and 5(b) that we have reproduced the dominant features and trends of the spectrum, although there are some differences in detail.

In offering some rationalization for our point of view in terms of proposed bilayer structures of the cyanobiphenyls, we show in Fig. 7 an illustration based upon one due to Leadbetter,[11] schematically representing the local structure in an 8*CB* layer in the S_A phase. Even in Leadbetter's figure[11] there is considerable tilting of the chains relative to the aligned aromatic portions.[22(b)] We have expanded on this to illustrate an idealized cooperative distortion mode of the chain regions which seems to preserve packing reasonably well. The internal rotational flexibility of the probe P would allow

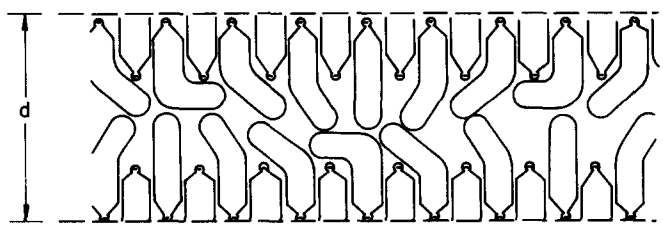

FIG. 7. Schematic two-dimensional representation of the molecular ordering in a cyanobiphenyl interpenetrating bilayer in the S_A phase. It is approximately to scale for 8CB (where $d \sim 29$ Å) (Ref. 11). Cyano groups are indicated by negative signs. The cooperative distortion mode of the aliphatic tails of the cyanobiphenyls that is discussed in the text is illustrated for each of the two layers of the bilayer but the variation from one molecule to the next is exaggerated for economy of space. Cooperativity between the distortion modes for each layer is indicated. The P probe is expected to be randomly substituted (in dilute solution) into the array such that its aromatic ring is aligned with the aromatic groups of the cyanobiphenyls, while the piperidine ring takes on the bent conformation characteristic of the aliphatic tails at that site.

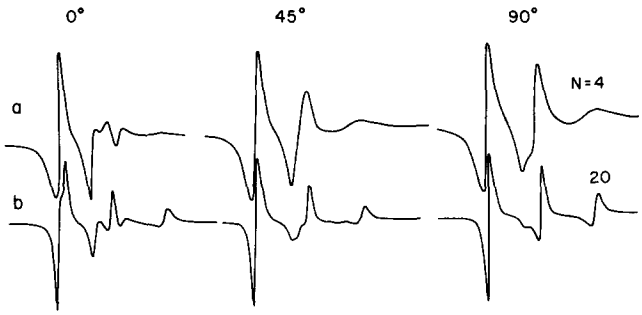

FIG. 8. Calculated ESR spectra with $\lambda = 3.5$, $\rho = -0.6$, $R_\perp = 3.8 \times 10^7\ s^{-1}$, $T_2^{*-1} = 0.7$ G and (a) $N = 4$ and (b) $N = 20$, and $P(\theta', \phi') \propto (\sin\theta')^{-1}$.

for the piperidine ring to take on various conformations relative to its own aromatic ring. We would to a first approximation presume that the piperidine ring lies in the chain region of the smectic bilayer and exhibits the same bent conformation relative to its own aromatic ring that is aligned with the aromatic groups of the cyanobiphenyl molecules. In this manner the piperidyl ring would report on the distribution function exhibited by the chain bends, consistent with our simulations. Finally, we note that both the stearamide and EOTA probes allow for such conformational variations of the piperidine ring relative to the rest of the molecule, while neither CSL nor PDT have this feature.[23(a)]

One aspect of our spectral analysis that might appear somewhat uncertain is the value of the diffusional asymmetry parameter N. In fact, it is not always the case that the slow motional spectra are particularly sensitive to this parameter.[23(b)] One might therefore think that in the present case, when we have a distribution of orientations (according to $P(\theta') = 1/\sin\theta'$) the dependence on N could be obscured. We illustrate in Fig. 8 that this is not the case. There we compare simulations [to be compared with the experimental spectrum in Fig. 5(a) for 20.5 °C] for $N = 4$ and $N = 20$. They clearly show the dramatic spectral changes resulting from a large change in N. We have varied N in integer steps from 1 to 10 as well as a number of larger values, and the spectral variations are such that we can assign an $N = 4 \pm 1$.

We did check whether a tilt of the primary diffusion (and ordering) axis z', relative to the magnetic z''' axis could improve agreement with experiment and found that it did not.

Since there are many parameters to vary in the simulations shown in Fig. 5(b), and the spectra are quite sensitive to all of them, we only sought reasonable approximations to the trends observed.

Another relevant set of parameters involves anisotropy in the viscosity (as distinct from anisotropic diffusion).[1,2] We have considered anisotropic viscosity in our simulations of P in 5*CB* discussed in the next section, where we also comment on this and related matters pertaining to improving the fits to the spectra of P in Fig. 5.

In summary, despite the distribution in the orientation of the director, we find that the various dynamic and ordering characteristics can be determined reasonably accurately. The dominant and unusual spectral features are, however, determined by the nature of the distribution function. Finally, the particular distribution function we used in our simulations in Fig. 5(b) [viz., $P(\theta') \propto 1/\sin\theta'$] at different T and θ has a simple feature in that it does not introduce *any* adjustable parameters into the fit, which is not true for other distributions.[1,3] Thus, its success or failure is readily judged. In the next section we do consider other types of distribution functions in some detail to provide a more critical assessment of our fits.

D. P in 5*CB*

5*CB* is a pure cyanobiphenyl liquid crystal that does not exhibit a smectic phase, but its nematic phase may be supercooled below its melting temperature of 24 °C. In view of the rather unusual results just described for P (and other probes) in *S*2, a comparative study of 5*CB* appeared useful. In order to perform orientation dependent studies, it was necessary to use electric-field alignment techniques, as discussed in Sec. II, to maintain the alignment of the director normal to the glass plates.

The results for P in 5*CB* are presented in Table IV and in Figs. 9–11. We find with 5*CB* that in the iso-

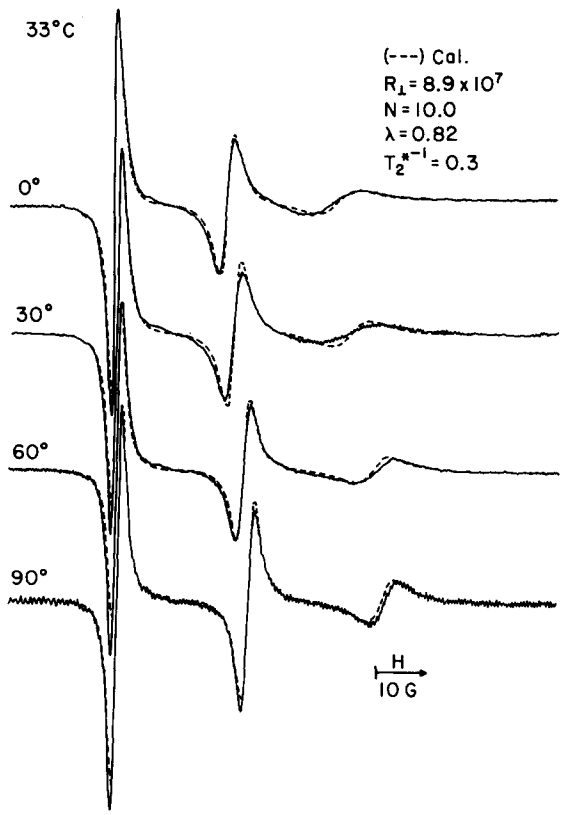

FIG. 9. (—) Experimental ESR spectra of 5×10^{-4} M P probe in 5*CB* contained between parallel glass plates about $200 \pm 10\,\mu$. thick in the presence of an electric field with $V = 280$ V at 33 °C and at orientations θ specified in the figure; (- - -) calculated spectra with $R_\perp$, λ, N, and T_2^{*-1} as denoted in the figure for the corresponding θ values.

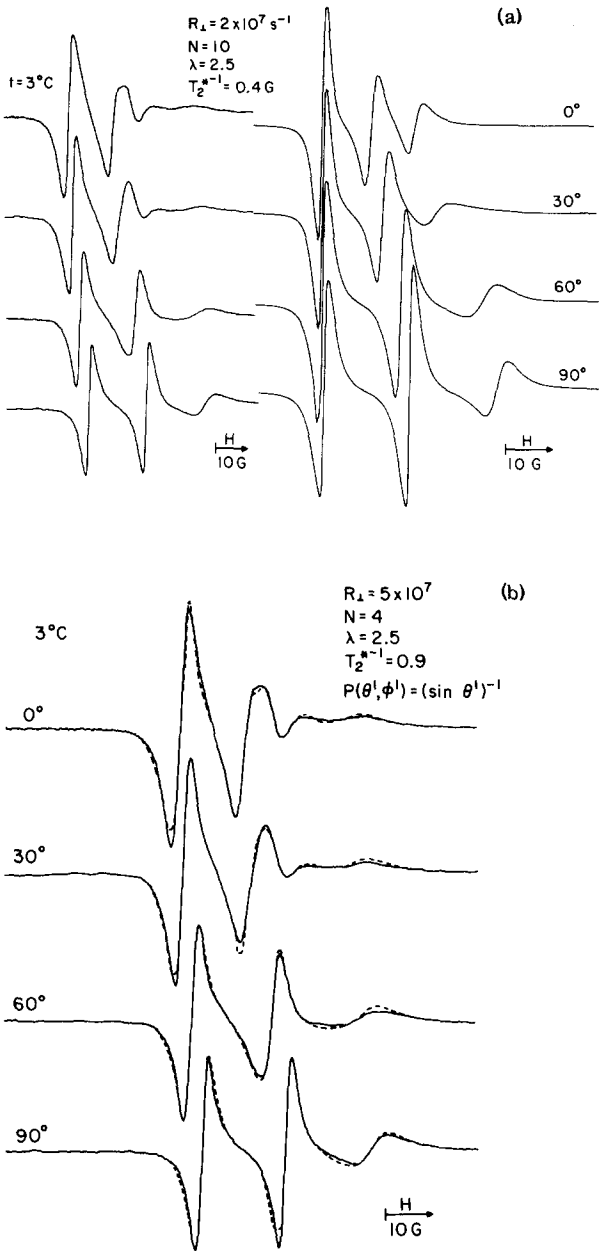

FIG. 10. (a) Experimental ESR spectra as in Fig. 9 except at 3 °C with the left-hand side series representing the experimental spectra and the right-hand side series the calculated spectra. (b) (- - -) calculated spectra with $R_\perp$, λ, N, and T_2^{*-1} as denoted in the figure and $P(\theta', \phi') \propto (\sin\theta')^{-1}$, (—) experimental ESR spectra from Fig. 10(a).

tropic phase $\tau_{\bar{R}}$ increases from 3.8×10^{-10} s at 54.5 °C to 8.9×10^{-10} s at 35.6 °C with an activation energy of (10.7 ± 1.0)/kcal/mol) or close to that for the isotropic phase of *S*2. In the nematic phase, near the $I \rightarrow N$ transition experimental spectra illustrated in Fig. 9 are obtained. The ESR spectra could be accurately simulated as illustrated in Fig. 9 for 33 °C, by gradually increasing λ and decreasing $R_\perp$ between 33 and 25 °C. This is consistent with typical nematic behavior. However, below 25 °C, the fit between the calculated and the experimental spectra became poor, as shown in Fig. 10(a) where the left-hand side series represents experimental spectra obtained at 3 °C and the right-hand series are illustrative spectra one would expect to observe at lower T for increased ordering and decreased rotational rates. On the other hand, the low T experimental line shapes in Fig. 10(a) are quite similar to the ESR spectra of P in the S_A phase of *S*2 [cf. Fig. 5(a), the 20–30 °C range]. This suggests that they be fit with the $P(\theta') \propto 1/\sin\theta'$ distribution. We illustrate in Fig. 10(b) the good fit obtained in this way. Furthermore, the $E_{act} \sim 4$ kcal/mol estimated for the supercooled region is a low value (but not quite as low as the S_A phase of *S*2), implying the dynamics of P are largely dominated by the dynamics of the alkyl-chain modes.[1(b)] Also, essentially the same value of $N \approx 4$ is obtained as for the S_A phase of *S*2.

It seems reasonable to suppose that in the supercooled nematic phase of 5*CB* the short-range packing of the 5*CB* molecules increases and is becoming rather similar to the S_A phases exhibited by *S*2 (and other members of this family of liquid crystals such as 8*CB*, cf. Fig. 1) which exhibit a true S_A phase. That is, the 5*CB* molecules are packing in interpenetrating layers. This has been suggested in recent x-ray studies on cyanobiphenyls.[22(b),24] Thus, a similar mechanism, such as the one of cooperative chain distortions (cf. Fig. 7) would be expected to occur also.

We cannot say much about such a mechanism in the normal nematic region (33–25 °C), because the ordering is too weak to distinguish whether or not the $1/\sin\theta'$ distribution is needed.

It was possible to obtain reproducible orientation-dependent spectra at a lower temperature of −1 °C, which is considerably changed in appearance from the one at +3 °C [cf. Fig. 11(a)]. Again we used the $1/\sin\theta'$ distribution to simulate the spectra, but we could not obtain as satisfactory a fit as at +3 °C. The discrepancies between theory and experiment are similar to those seen for *S*2 solvent [cf. Fig. 5(b) vs Fig. 5(a)] but more pronounced. In fact, there is a close similarity between such discrepancies and ones first seen by Polnaszek and Freed in their study of PD-tempone in phase V solvent[1(a)] (cf. their Fig. 13, where the theoretical low-field line is consistently too sharp and intense compared to the experimental one with a less pronounced discrepancy for the broader high-field line). In that case partial success in improving agreement was obtained by introducing an anisotropy in the viscosity. We therefore performed simulations with the addition of anisotropic viscosity according to formulas in Refs. 2 and in Appendix A. Our best fit with an $\hat{N} \equiv \hat{R}_\parallel / R_\perp = 1.5$ is shown in Fig. 11(b) (here $\hat{R}_\parallel$ is the component of the diffusion tensor along the director axis, while $\hat{R}_\perp = R_\perp$ is its value perpendicular to this axis). The considerably poorer fit obtained with no anisotropy in viscosity (i.e., $\hat{N} = 1$) is also shown. We found that with the addition of an $\hat{N} \neq 1$ the fit became considerably more sensitive to the value of λ used, and now we had to use a smaller value of $\lambda = 1.5$ to optimize the fit.

Polnaszek and Freed[1(a)] obtained even better simulations by introducing a very approximate "fluctuating torque model" and then argued that fluctuations in the local structure parameter (e.g., SRLS) are likely a

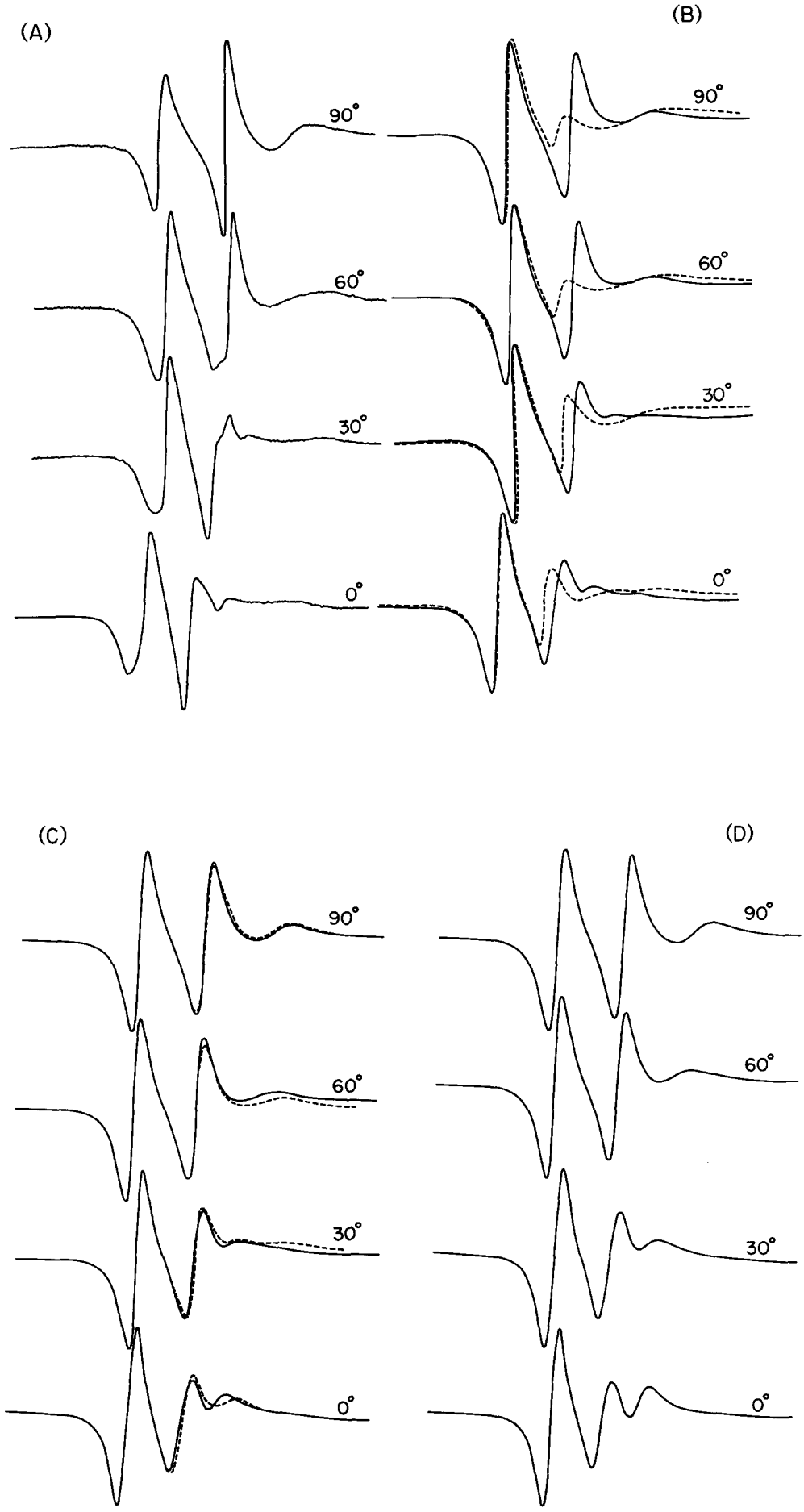

FIG. 11. (A) Experimental ESR spectra as in Fig. 10(a) except at $-1\,^{\circ}C$; (B) Calculated ESR spectra: (—) with $\lambda = 1.5$, $\rho \approx 0$, $R_{\perp} = 2.5 \times 10^7\ s^{-1}$ $T_2^{*-1} = 1.5$ G, $N = 4$, and $\hat{N} = 1.5$; (- - -) with the same parameters except that $\hat{N} = 1.0$ corresponding to no anisotropy in viscosity Both cases are for $P(\theta', \phi') \propto (\sin\theta')^{-1}$ (C) Same as (B) (with $\hat{N} = 1.5$) except that (—) corresponds to the mixed distribution (cf. text) and (- - -) corresponds to random distribution (cf. text). (D) Same as (B) (with $\hat{N} = 1.5$) except that distorted $(\sin\theta')^{-1}$ distribution is used with $k^2 = 0.99$ (cf. text).

better representation of the physical situation, and subsequent work has been supportive of this suggestion [cf. Refs. 1(b), 2(a), and 3(a)]. We therefore suspect that these anomalies, apparent from our simulations of the $-1\,^{\circ}C$ spectra, are again symptomatic of a SRLS mechanism. [We have not performed related simulations in the present work, since we have yet to incorporate these models (or better versions) into the already complex theory (given in the Appendix) required to analyze our orientation-dependent spectra.] What this would imply is that there must be local *dynamic* cooperativity between reorientation of the piperidyl ring and reorientations, flexing motions, etc. of the alkyl chains of the 5*CB* molecules which surround the piperidyl ring. This dynamic cooperativity would be distinct from and superimposed upon the effects, static on the ESR time scale, leading to the presumed $1/\sin\theta'$ distribution of chain directors [the $\hat{n}_i^c(r)$] about which the chains reorient, flex, etc. The similar discrepancies observed in Fig. 5(a) vs Fig. 5(b) would imply that a similar mechanism (e.g., SRLS) is also present in the S_A phase of *S*2 solvent.

We also explored whether the comparison between experiment and theory could be improved by modifying the distribution function $P(\theta', \phi')$, and some of our results (corresponding to best fits from each type of model) are shown in Figs. 11(c) and 11(d). Figure 11(c) shows the effect of letting $P(\theta', \phi') \propto (\sin\theta)^{-1} \exp[+\hat{\lambda} P_2(\theta')]$ [where $P_2(\theta') = D^2_{0,0}(0, \theta', 0) = \frac{1}{2}(3\cos^2\theta' - 1)$] with $\lambda = 2$. This mixed model introduces some additional alignment potential favoring the $\theta' = 0^{\circ}$ (or untilted) orientation. It is compared with predictions with $P(\theta', \phi') \propto \exp[+\hat{\lambda} P_2(\theta')]$, i.e., a random or Boltzmann-type of distribution. Figure 11(d) shows the effect of letting

$$P(\theta', \phi') = (\sin\theta')^{-1}(1 - k^2\cos^2\theta')^{-1/2} \Big/ \int_0^{\pi} (1 - k^2\cos^2\theta')^{-1/2} d\theta' ,$$

with $k^2 = 0.99$, corresponding to a distorted cooperative mode that favors the $\theta' = 0^{\circ}$ orientation. (This form is suggested by the form obtained in a different case, that of cholesterics, where high magnetic fields distort the helical pitch.[25(a)] In the present case, it would imply that packing forces within the layers tend to reduce the possibility of large tilt angles of the chains, which would appear to be reasonable physically.)[25(b)] We can summarize our results by noting that the best overall fit for all tilt angles is with $P(\theta', \phi') \propto (\sin\theta)^{-1} \times \exp[+2P_2(\theta')]$, while the best fits at $\theta = 0^{\circ}$ and 90° are, respectively, with $P(\theta', \phi') \propto (\sin\theta')^{-1}$ and with the distorted mode ($k = 0.99$). In all these cases and $\hat{N} = 1.5$ was significantly better than $\hat{N} = 1$. We thus conclude that the primary improvements to the spectral fits for P in 5*CB* are the introduction of the $(\sin\theta')^{-1}$ distribution and the anisotropy in viscosity, although some further improvements can be achieved with modifications of the $(\sin\theta')^{-1}$ distribution.

Similar simulations for P in *S*2 show that comparable improvements are realized by using an $\hat{N} = 1.5$ and the same modifications of the $(\sin\theta')^{-1}$ distribution.

Finally, we return to the matter of the considerably different results for the magnetic parameters of P in 5*CB* vs *S*2 solvent that are given in Table I. It turns out, from careful analysis of the spectra of P in 5*CB* in the isotropic phase that $a_N = 15.70$ G or just the value from the rigid limit magnetic parameters of P in *S*2 (rather than the considerably larger value of 16.93 G from the values for P in 5*CB*). Thus we used the magnetic parameters of P in *S*2 to analyze the higher temperature nematic spectra of P in 5*CB*. At the lower temperatures, where the lines are broader, we found the spectra were not very sensitive to which set of parameters were used (i.e., requiring only small adjustments in λ, $R_{\parallel}$, $R_{\perp}$, etc., which were insignificant compared to the large discrepancies discussed above), so that the question of which set of parameters to use had little bearing on the discussion above. Significant changes in magnetic parameters of this order occurring in different solvent phases were previously reported by Meirovitch and Freed [Ref. 3(b)] for lipid probes 7, 6-PC, and 12-doxylstearic acid in the high-temperature $L_{\alpha}(1)$ lamellar phase vs the low-temperature biaxial phase, and were suggested as likely due to packing effects in the biaxial phase which might cause bending or otherwise distort the nitroxide moiety. This interpretation seems consistent with our above model of the bending of the piperidine ring of P vs its aromatic region in the low temperature regions where the cooperative distortion mode manifests itself. The difference in rigid-limit parameters measured in *S*2 vs 5*CB* solvent may just reflect differences in structure of the microcrystallites in the mixed solvent with longer chains (i.e., *S*2) vs 5*CB*, a matter for further study.[25(c)]

IV. SUMMARY AND CONCLUSIONS

We have in this work emphasized detailed spectral simulation based upon well-defined molecular models of the dynamic structure of liquid crystals containing solute probes. It was illustrated how comparison of such simulations with experimental spectra are the most reliable means of interpretation.

We found distinctly different structural and dynamic behavior for the flexible probe P in the smectic (or supercooled nematic) phases of benzilidene derivative liquid crystal (40, 6) with monolayer structure vs cyanobiphenyls (*S*2 and 5*CB*) with bilayer structure. Thus, we infer from the present results for P as well as by comparison with previous studies with other probes that:

(1) The motion of P in the various isotropic and nematic phases is quite similar and characterized by substantial anisotropy of rotation $N \approx 6$–10 consistent with a similar extended conformation of P and/or freedom for internal rotation of the piperidine ring in both these phases. This is consistent with a similar local dynamic structure in both phases, although only in the nematic phase is there a nonzero mean ordering that is characteristic of this phase. For P (more precisely the piperidine ring) this mean ordering appears to be close to axially symmetric.

(2) In the various smectic phases the ordering of the piperidine ring loses its near-axial symmetry (a fea-

ture that could be distinguished from other interpretations only by careful simulation of the orientation-dependent spectra) presumably because of greater cooperativity of the piperidine ring with adjacent functional groups.

(3) For the benzilidene 40, 6 the $N-S_A$ phase-change reduces $R_\perp$ with $R_\parallel$ remaining about the same, while for the S_A-S_B phase change, $R_\perp$ remains constant and $R_\parallel$ decreases by a substantial amount. This is interpreted as (a) increased packing in the central core region in the S_A phase leading to greater frictional resistance to reorientation of the long molecular axis, but relative freedom for internal rotation of functional groups and (b) greater cooperativity of reorientation of functional groups in the hexagonal close-packed S_B phase, hence the reduced rate of internal motion of the piperidine ring. A partial freezing of the alkyl chain motions in the S_B phase has been invoked to explain the rapid motion of the small PDT probe in terms of fairly well-developed clathrates or holes in the chain region.

(4) P in the S_A phase of the cyanobiphenyl mixed solvent $S2$ shows unusual orientation-dependent spectral features which could be satisfactorily interpreted in terms of the two-dimensional distribution function $[P(\theta', \phi') \propto 1/\sin\theta']$ for the local director experienced by the piperidine ring although no such features are found for the rigid CSL probe. Furthermore, the extremely low activation energy ($E_a \approx 1.5$ kcal/mol) for P (only in this phase) can be interpreted, based upon past work, as due to the dynamics of P being dominated by interaction with alkyl chains vs the rigid aromatic core. Thus, the anomalous observations are interpreted as cooperative chain distortions in this bilayer S_A, which through intermolecular packing forces leads to a coherent distribution of orientations of the piperidine ring, that tends to pack in the alkyl region of the bilayer in this phase.

(5) In the supercooled nematic phase of the cyanobiphenyl $5CB$, similar unusual spectral features are found for P consistent with the model that local smectic (bilayer) ordering is occurring even though there is no long-range smectic order, and this ordering exhibits the "coherent" chain distortions sensed by the piperidine ring. Detailed comparison of experimental and simulated spectra shows evidence for anisotropic viscosity which might alternatively be explained by a SRLS mechanism implying *dynamic* cooperativity of the reorientation of the piperidine ring in the presence of the dynamic fluctuations of the surrounding chains, and this is probably also the case for P in the S_A phase of $S2$ solvent.

(6) In general, the approach of comparing results from a variety of different probes permits a more detailed interpretation of the dynamic structure of liquid crystalline phases, and more experiments along these lines may be expected to further clarify the phenomena explored here.

APPENDIX A: GENERAL EXPRESSIONS FOR ESR SIMULATIONS

Introduction

In this appendix we describe the expressions that we used to calculate the ESR spectra. The formulation is appropriate for:

(1) Any value of the single nuclear spin I and a single electron spin: $S = 1/2$.

(2) A potential given by the equation[16]

$$U/kT \propto \sum_{L,K}{}' \lambda_K^L D_{0K}^L(\Omega) ,$$

where the summation is taken for L, $K = 0, \pm 2, \pm 4$, and $\lambda_K^L = \lambda_{-K}^L$, which are dimensionless expansion coefficients, while the $D_{0K}^L(\Omega)$ are the generalized spherical harmonics (also called the Wigner rotation matrix elements).

(3) A molecular tilt (diffusion, **g**, and **A** tensors do not necessarily have the same system of principal axes).

(4) A director tilt (i.e., different directions of the static field and the director).

Also no restriction is placed on the magnitude of the magnetic field.

The programs we developed are specifically written for the PDP 11/34 minicomputer, and they use the Lanczos algorithm (L.A.) in order to achieve tridiagonal form [cf. Ref. 12(c) for a general description of the L.A.; cf. also Ref. 26 for specific information about the computer implementation of the algorithm].

Matrix elements for the complete problem (all values of magnetic field)

In this section we shall derive the matrix elements associated with the full ESR problem. Hereafter we shall use the Rose convention for the Wigner rotation matrices.[27,28]

The ESR absorption spectrum can be written as

$$I(\omega) = \frac{1}{\pi} \operatorname{Re}\{\langle v | [i(\omega \mathbf{1} - \mathbf{L}) + \mathbf{\Gamma}]^{-1} | v \rangle\} , \tag{A1}$$

where $\mathbf{\Gamma}$ is the symmetrized diffusion operator and $\mathbf{L}$ is the Liouville operator associated with the Hamiltonian of the magnetic interactions and $|v\rangle$ is the unit vector of the *allowed* ESR transitions in the Liouville space discussed below (cf. also subsection c). We assume the following Hamiltonian (in angular frequency units)[29]:

$$H = \frac{\beta_e}{\hbar} \mathbf{B}_0 \cdot \mathbf{g} \cdot \mathbf{S} + \gamma_e \mathbf{I} \cdot \mathbf{A} \cdot \mathbf{S} , \tag{A2}$$

where it is assumed that the nuclear Zeeman interactions are negligible. The operators $\mathbf{L}$ and $\mathbf{\Gamma}$ are defined in the Liouville space of the product of the normalized Wigner rotation matrices and the spin *transitions*:

$$|m^{s'} m^{I'}; m^{s''} m^{I''}; LMK\rangle \equiv |m^{s'} m^{I'}; m^{s''} m^{I''}\rangle \sqrt{\frac{2L+1}{8\pi^2}} D_{MK}^L(\Omega) , \tag{A3}$$

where m^S and m^I are the eigenstates of the z components of the electronic spin operator **S** and of the nuclear spin operator **I**, respectively:

$$S_z|m) = m|m) \ , \tag{A4a}$$

$$I_z|m^I) = m^I|m^I) \ ; \tag{A4b}$$

Here we distinguish between kets in ordinary spin space by: $|\sim)$ from kets in Liouville space by: $|\sim\rangle$. Note that the space of the electron spin transitions is constructed according to the following rule, where the matrix element of S in spin space is rewritten as a scalar product in Liouville space:

$$(m^{S'}|\mathbf{S}|m^{S''}) \rightarrow \langle \mathbf{S}|m^{S'}, m^{S''}\rangle \ . \tag{A5}$$

That is, $|m^{S'} m^{S''}\rangle$ becomes a ket representing the electron-spin transition. The same holds for the nuclear spin transitions.

The reference frames for the problem are

(L) Laboratory frame (x, y, z): z axis parallel to $\mathbf{B}_0$.

(d) director frame (x'', y'', z''): z'' axis parallel to **d**, where **d** defines the axis of symmetry for an uniaxial liquid crystal

(D) Diffusion frame (x', y', z'): principal axes of the diffusion tensor **R**.

(g) g-tensor frame: principal axes of the g tensor

(A) A-tensor frame: principal axes of the A tensor

$\Big\}\ (x''', y''', z''')$.

We take as the argument Ω of the Wigner rotation matrices $D^L_{MK}(\Omega)$ the Euler angles that define the transformation from the (d) frame to the (D) frame

$$\Omega \equiv \Omega_{d\text{-}D} \ . \tag{A6}$$

[Therefore the α angle in $\Omega \equiv (\alpha, \beta, \gamma)$ represents the rotation around z''.] With this choice for Ω, the nonzero components of $|v\rangle$ are reduced to a minimum.

Matrix elements of **L**

We write the Hamiltonian in the spherical tensor notation as

$$H = \sum_{\mu, l, m} F^{(l,m)}_{\mu,L} * A^{(l,m)}_{\mu} \ , \tag{A7}$$

where μ specifies the kind of interaction (Zeeman or hyperfine) and $A^{(l,m)}_{\mu}$ are the spherical components of the spin operators in the (L) frame. Hereafter, the index η in $F^{(l,m)}_{\mu,\eta}$ defines the reference frame in which the spherical components of the tensor μ are calculated. By means of the transformation property of the spherical components of a tensor:

$$F^{(l,m)}_{\mu,1} * = \sum_{m'} D^l_{m,m'}(\Omega_{1\text{-}2}) F^{(l,m')}_{\mu,2} * \ , \tag{A8}$$

we can write explicitly the dependence of H on the orientation of the molecule:

$$H = \sum_{\substack{\mu, l, m \\ m', m''}} d^l_{m,m'}(\psi)\, D^l_{m',m''}(\Omega) F^{(l,m'')}_{\mu,D} * A^{(l,m)}_{\mu} \ , \tag{A9}$$

where ψ defines the angles between **d** and $\mathbf{B}_0$,[27–29] and $d^l_{m,m'}(\psi) = D^L_{m',m''}(0, \psi, 0)$.

In order to have simple equations for the matrix elements, the indices for the transitions are redefined according to the following rules:

$$p^i = m^{i'} - m^{i''} \ , \quad p^S = -1, \ 0, \ 1 \ , \quad p^I = -2I, \ -2I+1, \ldots, 2I \ , \tag{A10a}$$

$$q^i = m^{i'} + m^{i''} \ , \quad q^i = -Q^i, \ -Q^i+2, \ldots, Q^i \ , \quad Q^s = 1 - |p^S| \ , \quad Q^I = 2I - |p^I| \ , \tag{A10b}$$

with $i = S$ or $i = I$. In Appendix B the matrix elements of $(A^{(l,m)}_{\mu})^x$ are calculated.

We can now write the matrix elments of **L** as

$$\langle p^S_1 q^S_1; p^I_1 q^I_1; L_1 M_1 K_1|\mathbf{L}|p^S_2 q^S_2; p^I_2 q^I_2; L_2 M_2 K_2\rangle = N_L(L_1 L_2)(-1)^{M_1+K_1} \sum_{\mu, l} \langle p_1 q_1; p^I_1 q^I_1|[A^{(l,\Delta p)}_{\mu}]^x|p^S_2 q^S_2; p^I_2 q^I_2\rangle \times d^l_{\Delta p, M_1 - M_2}(\psi) F^{(l,K_1-K_2)} * \begin{pmatrix} L_1 & l & L_2 \\ M_1 & M_2 - M_1 & -M_2 \end{pmatrix} \begin{pmatrix} L_1 & l & L_2 \\ K_1 & K_2 - K_1 & -K_2 \end{pmatrix} , \tag{A11}$$

where $N_L(L_1, L_2) = (2L_1+1)^{1/2}(2L_2+1)^{1/2}$ and $\Delta p = p^S_1 + p^I_1 - p^S_2 - p^I_2$. Equation (B9) leads to the following symmetry relation:

$$\langle -p^S_1, q^S_1; -p^I_1, q^I_1; L_1, -M_1, -K_1|\mathbf{L}|-p^S_2, q^S_2; -p^I_2, g^I_2; L_2, -M_2, -K_2\rangle = (-1)^{1+M_1+M_2+K_1+K_2} \langle p^S_1, q^S_1; p^I_1, q^I_1; L_1, M_1, K_1|\mathbf{L}|p^S_2, q^S_2; p^I_2 q^I_2; L_2, M_2, K_2\rangle \ . \tag{A12}$$

From Eq. (B9) one may derive that in absence of director tilt (i.e., $\psi = 0°$), **L** is factored into blocks corresponding to the linear combination of the indices:

$$p^S + p^I - M = \text{const.} \tag{A13}$$

Matrix elements of Γ

The operator Γ includes all the sources of relaxation of the system. One may implement different models for this process, specifically:

(i) Γ_{iso}: isotropic rotational diffusion in liquids,

(ii) Γ_U: rotational diffusion correction for liquid crystals,

(iii) Γ_{dj}: discrete jumps among equivalent sites,

(iv) Γ_{ex}: Heisenberg spin exchange.

The overall Γ operator is taken as a superposition of these processes:

$$\Gamma = \Gamma_{iso} + \Gamma_U + \Gamma_{dj} + \Gamma_{ex} . \tag{A14}$$

In the following part we shall examine one by one these contributions.

The specific form for Γ_{iso} describes reorientational motion in isotropic liquids according to the following equation for its matrix elements:

$$\langle L_1 M_1 K_1 | \Gamma_{iso} | L_2 M_2 K_2 \rangle = \delta_{L_1,L_2}\delta_{M_1,M_2}\delta_{K_1,K_2}\{R_\perp L_1(L_1+1)[1+\tau_\perp R_\perp L_1(L_1+1)]^{-E_\perp} + K_1^2[R_\parallel(1+\tau_\parallel R_\parallel K_1^2)^{-E_\parallel} - R_\perp(1+\tau'_\perp R_\perp K_1^2)^{-E'_\perp}]\} . \tag{A15}$$

The diffusion motion is considered axial and the model dependence of each degree of freedom is treated independently. (We mention that a different model for the perpendicular and the parallel motion is justified in the case of superposition of a slow overall motion and a fast internal motion.[30]) The possible limiting situations are[29]

(i) Brownian motion: $\tau = 0$, $E = 0$;

(ii) free diffusion: $\tau \neq 0$, $E = 1/2$;

(iii) jump diffusion: $\tau \neq 0$, $E = 1$.

Anisotropic viscosity[1,2(a)] is also included by adding the diagonal term $(\hat{R}_\parallel - R_\perp)M_1^2$ to Eq. (A15).

The diffusion operator for a liquid crystal (Γ_{LC}) is given by the symmetrized Smoluchowski equation[29]:

$$\Gamma_{LC} = \left[J - \frac{1}{2kT}(JU)\right] R \left[J + \frac{1}{2kT}(JU)\right] , \tag{A16}$$

where J is the angular momentum operator, U is the mean potential acting on the molecule, and R is the rotational diffusion tensor of the molecule. The equilibrium distribution probability is written as

$$P(\Omega) = \exp\{-U/kT\} \Big/ \int d\Omega \exp\{-U/kT\} . \tag{A17}$$

The operator Γ in Eq. (A16) can be rewritten as

$$\Gamma_{LC} = \Gamma_{iso} + \Gamma_U , \tag{A18}$$

where Γ_{iso} is its isotropic part already contained in Eq. (A15) for $\tau_\perp = \tau'_\perp = \tau_\parallel = 0$, and Γ_U is the new contribution:

$$\Gamma_U = \frac{1}{2kT}\{R_\perp(J^2U) + (R_\parallel - R_\perp)(J_z^2U)\} - \frac{1}{4k^2T^2}\{R_\perp(J_+U)(J_-U) + R_\parallel(J_zU)^2\} . \tag{A19}$$

We assume the following form for the potential:

$$U = -kT \sum_{L,K}{}' \lambda_K^L D_{0K}^L(\Omega) , \tag{A20}$$

where the summation is restricted to the values 0, ± 2, ± 4 for the indices L and K and the coefficients λ_K^L have the property[29]:

$$\lambda_K^L = \lambda_{-K}^L = \lambda_K^{L*} . \tag{A21}$$

We note that the use of a potential explicitly dependent on γ (i.e., at least some λ_K^L for $K \neq 0$ are different from zero) implies that the diffusion frame is not axially symmetric, since a rotation around the z' axis of the (D) frame changes the functional dependence of U on γ. The operator Γ_U can be written as

$$\Gamma_U = \sum_{L,K} X_K^L D_{0K}^L , \tag{A22}$$

where the coefficients X_K^L are

$$X_K^L = -\tfrac{1}{2}\lambda_K^L\{R_\perp L(L+1) + K^2(R_\parallel - R_\perp)\} - \sum_{L_1,K_1}\sum_{L_2,K_2}(2L+1)\lambda_{K_1}^{L_1}\lambda_{K_2}^{L_2}\begin{pmatrix} L_1 & L & L_2 \\ 0 & 0 & 0 \end{pmatrix}\Big\{R_\perp[L_1(L_1+1) - K_1(K_1+1)]^{1/2} \times [L_2(L_2+1) - K_2(K_2-1)]^{1/2}\begin{pmatrix} L_1 & L & L_2 \\ K_1+1 & -K & K_2-1 \end{pmatrix} + R_\parallel K_1 K_2 \begin{pmatrix} L_1 & L & L_2 \\ K_1 & -K & K_2 \end{pmatrix}\Big\} . \tag{A23}$$

The matrix elements of Γ_U are

$$\langle L_1 M_1 K_1 | \Gamma_U | L_2 M_2 K_2 \rangle = \delta_{M_1 M_2} \sum_L X_{K_1-K_2}^L N_L(L_1, L_2)(-1)^{K_1+M_1}\begin{pmatrix} L_1 & L & L_2 \\ M_1 & 0 & -M_1 \end{pmatrix}\begin{pmatrix} L_1 & L & L_2 \\ K_1 & K_2-K_1 & -K_2 \end{pmatrix} . \tag{A24}$$

The program also allows a discrete jump model among equivalent sites[31] in the particular case that these sites are connected by a rotation around one molecular axis (namely the z' axis). The matrix elements of Γ_{dj} are

$$\langle L_1 M_1 K_1 | \Gamma_{dj} | L_2 M_2 K_2 \rangle = \delta_{L_1 L_2}\delta_{K_1 K_2}\delta_{M_1 M_2}\frac{1}{\tau_{dj}}(1 - \delta_{K_1}^{n_s}) , \tag{A25}$$

where τ_{dj} is the mean time between jumps, n_s is the number of equivalent sites and δ_K^n is defined as

$$\delta_K^n = \begin{cases} 1, & \text{if } K \text{ is a multiple of } n , \\ 0, & \text{otherwise} . \end{cases} \tag{A26}$$

Last we have the spin exchange operator Γ_{ex}. It is assumed that the lifetime of radical-pair encounters is much shorter than the time scale associated with the

rotational diffusion process, i.e., τ_R and much shorter than the effective exchange time (i.e., ω_{HE}^{-1} see below). Also Γ_{ex} is assumed to be independent of the orientation of the radicals, so its matrix elements are[5,32]

$$\langle p_1^S q_1^S; p_2^I q_1^I | \Gamma_{ex} | p_2^S q_2^S; p_2^I q_2^I \rangle = \omega_{HE} \delta_{p_1^S p_2^S} \delta_{p_1^I p_2^I} \{ \delta_{q_1^S, q_2^S} \delta_{q_1^I, q_2^I} - \tfrac{1}{2} \delta_{p_1^S,0} \delta_{q_1^I, q_2^I} - (2I+1)^{-1} \delta_{p_1^I,0} \delta_{q_1^S, q_2^S} \} , \quad \text{(A27)}$$

where ω_{HE} is the effective spin exchange frequency.

Components of the starting vector

The starting vector for ESR problems is defined in terms of the normalized vector associated with $|S_x P^{1/2}(\Omega)\rangle$.[29,33(a)] Therefore, its components in the basis set defined by Eqs. (A3) and (A10) are

$$|v\rangle = 2^{-1/2} (|v_1\rangle + |v_{-1}\rangle) , \quad \text{(A28)}$$

$$\langle p^S q^S; p^I q^I, LMK | v_m \rangle = (2I+1)^{-1/2} \delta_{p^I,0} \delta_{p^S,m} \delta_{M,0} \times \sqrt{\frac{2L+1}{8\pi^2}} \int d\Omega D_{0K}^{L*} P^{1/2}(\Omega) , \quad \text{(A29)}$$

where the integral over Ω is different from zero only for even L and K since from the definition (A20) of U, the probability $P(\Omega) = P(\beta, \gamma)$ has the following symmetry properties:

$$P(\beta, \gamma) = P(\beta, -\gamma) = P(\beta, \pi - \gamma) = P(\pi - \beta, \gamma) . \quad \text{(A30)}$$

The number of components of $|v\rangle$ can be decreased in the absence of director tilt, by making use of the symmetry properties of the matrices involved with respect to the change of sign in the indices p^S, p^I, K, and M. This can be easily derived by means of the matrix Y defined as

$$\langle p_1^S q_1^S; p_1^I q_1^I; L_1 M_1 K_1 | Y | p_2^S q_2^S; p_2^I q_2^I; L_2 M_2 K_2 \rangle = \delta_{-p_1^S, p_2^S} \delta_{q_1^S, q_2^S} \delta_{-p_1^I, p_2^I} \delta_{q_1^I, q_2^I} \delta_{L_1, L_2} \delta_{-M_1, M_2} \delta_{-K_1, K_2} (-1)^{M_1 + K_1} . \quad \text{(A31)}$$

This matrix has the following properties:

$$Y^2 = 1 , \quad \text{(A32a)}$$

$$Y |v_m\rangle = |v_{-m}\rangle , \quad \text{(A32b)}$$

$$Y L Y = -L^* , \quad \text{(A32c)}$$

$$Y \Gamma Y = \Gamma , \quad \text{(A32d)}$$

where Eq. (A32c) is derived from Eq. (A12), and Eq. (A32d) can be easily demonstrated from Eqs. (A15), (A24), (A25), and (A27). The formal expression (A1) of the spectrum can be rewritten as

$$I(\omega) = \frac{1}{2} \sum_{m,m'} I_{m,m'}(\omega), \quad m, m' = \pm 1 , \quad \text{(A33)}$$

where

$$I_{m,m'}(\omega) = \frac{1}{\pi} \mathrm{Re} \langle v_m | [i(\omega - L) + \Gamma]^{-1} | v_{m'} \rangle . \quad \text{(A34)}$$

From Eqs. (A32) it is demonstrated that

$$I_{m,m'}(\omega) = -I_{m,-m'}(-\omega) . \quad \text{(A35)}$$

We can now distinguish two cases:

(i) ESR spectrum without director tilt ($\psi = 0°$). In this case $I_{-1,1}(\omega) = 0$ as a consequence of Eq. (A13). Ultimately the spectrum can be written as

$$I(\omega) = \tfrac{1}{2} [I_{11}(\omega) + I_{11}(-\omega)] . \quad \text{(A36)}$$

This implies that the calculation can be done with $|v_1\rangle$ as starting vector and only at the end is it necessary to symmetrize the spectrum with respect to ω. We mention that the change of the starting vector from $|v\rangle$ to $|v_1\rangle$ is of major importance in reducing the size of the matrix to be diagonalized, since in this way the basis elements with $p^S \neq 1$ can be very efficiently truncated.

(ii) ESR spectrum with director tilt ($\psi \neq 0$). Since in this case $I_{-1,1}(\omega)$ is different from zero and since the Lanczos algorithm is efficiently applied when the right- and left-hand vector are equal,[12] one needs to use the full starting vector $|v\rangle$ as given in Eq. (A26).

Symmetrization of L

Since the Lanczos algorithm can be applied when the matrix associated with $-iL$ is complex symmetric, we must introduce a proper transformation of the basis set, so that the operator L has only real matrix elements. The new basis set is defined as

$$|p^S q^S; p^I q^I; LMKj^K\rangle = [2(1+\delta_{K,0})]^{-1/2} \exp\left\{ i \frac{\pi}{4} (1 - j^K) \right\} \times |p^S q^S; p^I q^I\rangle (|LMK\rangle + j^K (-1)^{L+K} |LM-K\rangle) , \quad \text{(A37)}$$

where the K index now has only positive values and the allowed values for j^K are

$$K \neq 0 , \quad j^K = \pm 1 ,$$

$$K = 0 , \quad j^K = (-1)^L , \quad \text{(A38)}$$

The starting vector Γ_V and L in this new representation are, respectively,

$$\langle p^S q^S; p^I q^I; LMKj^K | v_m \rangle = \delta_{m,p^S} \delta_{0,p^I} \delta_{0,M} \delta_{1,j^K} (2I+1)^{-1/2} \times [2/(1+\delta_{K0})]^{1/2} \int d\Omega P(\Omega)^{1/2} \mathrm{Re}\{D_{0K}^L\} , \quad \text{(A39)}$$

$$\langle L_1 M_1 K_1 j_1^K | \Gamma_V | L_2 M_2 K_2 j_2^K \rangle = \delta_{M_1,M_2} \delta_{j_1^K, j_2^K} N(L_1, L_2) N_K(K_1, K_2) (-1)^{L_1 + M_1} \sum_L \begin{pmatrix} L_1 & L & L_2 \\ M_1 & 0 & -M_1 \end{pmatrix} \times \left\{ X_{K_1 - K_2}^L \begin{pmatrix} L_1 & L & L_2 \\ K_2 & K_2 - K_1 & -K_2 \end{pmatrix} + j_2^K (-1)^{L_2 + K_2} X_{K_1 + K_2}^L \begin{pmatrix} L_1 & L & L_2 \\ K_1 & -K_1 - K_2 & K_2 \end{pmatrix} \right\} , \quad \text{(A40)}$$

$$\langle p_1^S q_1^S; p_1^I q_1^I; L_1 M_1 K_1 j_1^K \,|\, \mathrm{L} \,|\, p_2^S q_2^S; p_2^I q_2^I; L_2 M_2 K_2 j_2^K \rangle = N_L(L_1, L_2) N_K(K_1, K_2)(-1)^{M_1+K_1}$$
$$\times \sum_{\mu,l} \langle p_1^S q_1^S; p_1^I q_1^I | [A^{(l,\Delta p)*}] | p_2^S q_2^S; p_2^I q_2^I \rangle d^l_{\Delta p, M_1 - M_2}(\psi) \begin{pmatrix} L_1 & l & L_2 \\ M_1 & M_2 - M_1 & -M_2 \end{pmatrix} R_{\mu,l}(L_1 K_1 j_1^K; L_2 K_2 j_2^K) , \tag{A41}$$

where

$$R_{\mu,l}(L_1 K_1 j_1^K; L_2 K_2 j_2^K) = \begin{pmatrix} L_1 & l & L_2 \\ K_1 & K_2 - K_1 & -K_2 \end{pmatrix} G_{\mu,l}(j_1^K, j_2^K; K_1 - K_2) + j_2^K (-)^{L_2+K_2} \begin{pmatrix} L_1 & l & L_2 \\ K_1 & -K_2 - K_1 & K_2 \end{pmatrix} G_{\mu,l}(j_1^K, j_2^K; K_1 + K_2) , \tag{A42}$$

$$N_K(K_1, K_2) = (1 + \delta_{K_1,0})^{-1/2} (1 + \delta_{K_2,0})^{-1/2} , \tag{A43}$$

and the quantities $G_{\mu,l}$ are defined as

$$G_{\mu,l'}(j_1^K, j_2^K; K) = \delta_{j_1^K, j_2^K} \mathrm{Re}\{F_{\mu,D}^{(l,K)}\} + (1 - \delta_{j_1^K, j_2^K}) j_1^K \mathrm{Im}\{F_{\mu,D}^{(l,K)}\} \tag{A44}$$

and the spherical components $F_{\mu,D}^{(l,K)}$ can be written in terms of the principal values of the corresponding tensor μ according to the equations [cf. Eq. (A8)]

$$F_{g,D}^{(l,K)*} = \sum_m D^l_{K,m}(\Omega_{D\to g}) F_{g,g}^{(l,m)*} , \tag{A45}$$

$$F_{A,D}^{(l,K)*} = \sum_m D^l_{K,m}(\Omega_{D\to A}) F_{A,A}^{(l,m)*}$$
$$= \sum_{m,m'} D^l_{K,m}(\Omega_{D\to g}) D^l_{m,m'}(\Omega_{g\to A}) F_{A,A}^{(l,m)*} . \tag{A46}$$

Finally, we mention that the symmetries of a specific ESR problem allow one to reduce the size of the matrices. We consider, in particular, the following cases:

(i) Absence of director tilt ($\psi = 0$). Only the basis elements with

$$M = p^S + P^I - 1 \tag{A47}$$

are needed.

(ii) $\mathrm{Im}\{F_{\mu,D}^{(2,K)}\} = 0$. Only the basis elements with $j^K = 1$ are used. This is the case when the g and A tensors have the same principal axes and the molecular tilt is defined by only the polar angle:

$$\Omega_{D\to g} = \Omega_{D\to A} = (0, \beta, 0) . \tag{A48}$$

(iii) $F_{\mu,D}^{(2,\pm 1)} = 0$. Only the even values of index K are needed. This is the case when there is no molecular tilt.

(iv) $F_{\mu,D}^{(2,m)} = \delta_{m,0}$. In this case only the basis elements with even L and $K = 0$ are used. This corresponds to the situation of no molecular tilt and axial **g** and A tensors.

Matrix elements for the high-field problem

Under the conditions:

$$|\omega - \omega_0| \ll \omega_0 , \tag{A49a}$$

$$|A_{jj}| \ll B_0 , \tag{A49b}$$

$$|g_{jj} - \bar{g}| \gg \bar{g} , \tag{A49c}$$

where $\omega_0 = \bar{g}\beta B_0/\hbar$, the effect of the nonsecular terms can be treated perturbationally.[33(b)] By means of the Van Vleck formalism for perturbation theory,[34] the following equation for the absorption function is obtained:

$$I(\omega) = \frac{1}{\pi} \mathrm{Re}\{\langle v_\rho | [i(\omega \mathbf{1} - \mathrm{L}_\rho) + \Gamma_\rho]^{-1} | v_\rho \rangle\} , \tag{A50}$$

where now the problem is confined in the subspace defined by $p^S = 1$ and $q^S = 0$. Vector $|v_\rho\rangle$ and the matrix Γ_ρ are, respectively, the vector $|v_1\rangle$ and the matrix Γ considered in this subspace while L_ρ is defined as

$$\mathrm{L}_\rho = \mathrm{L}' + \frac{1}{\omega_0} \sum_m \mathrm{L}''_m (\mathrm{L}''_m)^{tr} , \tag{A51}$$

where L′ is the submatrix obtained from L for $p_1^S = p_2^S = 1$ $m = \pm 1$, and L''_m is the submatrix defined for $p_1^S = 1$, $p_2^S = 0$, $q_1^S = 0$, $q_2^S = m$.

At this stage it is convenient to introduce the transformation of the basis elements that takes into account the symmetry of the unperturbed Liouville submatrix L′. The following symmetry relation is derived from Eqs. (B7) and (B8b):

$$\langle 1, 0; -p_1^I, q_1^I | [A_\mu^{(l,-m)}]^\dagger | 1, 0; -p_2^I, q_2^I \rangle$$
$$= (-1)^{(p_1^I + p_2^I)} \langle 1, 0; p_1^I, q_1^I | [A_\mu^{(l,m)}]^\dagger | 1, 0; p_2^I, q_2^I \rangle . \tag{A52}$$

By substitution of this result into Eq. (A41) we obtain

$$\langle -p_1^I, q_1^I; L_1, -M_1, K_1, j_1^K | \mathrm{L}' | -p_2^I, q_2^I; L_2; -M_2, j_2^K \rangle = (-1)^{L_1+L_2+M_1+M_2} \langle p_1^I, q_1^I; L_1, M_1, K_1, j_1^K | \mathrm{L}' | p_2^I, q_2^I; L_2, M_2, K_2, j_2^K \rangle \tag{A53}$$

and a similar equation is derived for Γ_ρ. This suggests the following transformation of the basis set in which Γ_ρ and L′ are defined:

$$|p^I, q^I; L, M, K, j^M, j^K\rangle = [2(1 + \delta_{M,0}\delta_{pI,0})]^{-1/2} (|p^I, q^I; L, M, K, j^K\rangle + j^M (-1)^{L+M} |-p^I, q^I; L, -M, K, j^K\rangle) , \tag{A54}$$

where the indices $p^S = 1$ and $q^S = 1$ and $q^S = 0$ are implicit. In this new basis, the M index has only positive value and the allowed values for j^M are

$$j^M = \begin{cases} (-1)^L, & \text{for } p^I = M = 0 , \\ \pm 1, & \text{otherwise.} \end{cases} \tag{A55}$$

The matrix elements of L′ in this new basis set are

$$\langle p_1^I q_1^I; L_1 M_1 K_1 j_1^M j_1^K \,|\, \mathrm{L}' \,|\, p_2^I q_2^I; L_2 M_2 K_2 j_2^M j_2^K \rangle = \delta_{j_1^M, j_2^M} N_L(L_1, L_2) N_K(K_1, K_2) N_p(p_1^I M_1; p_2^I M_2)(-1)^{M_1+K_1}$$

$$\times \sum_{\mu, l} \Bigg\{ \langle 1, 0; p_1^I q_1^I | [A_\mu^{(l, p_1^I - p_2^I)}]^\times | 1, 0; p_2^I, q_2^I \rangle d^l_{p_1^I - p_2^I, M_1 - M_2}(\psi) \begin{pmatrix} L_1 & l & L_2 \\ M_1 & M_2 - M_1 & -M_2 \end{pmatrix} + j_2^M (-1)^{L_2 + M_2}$$

$$\times \langle 1, 0; p_1^I q_1^I | [A_\mu^{(l, p_1^I + p_2^I)}]^\times | 1, 0, -p_2^I, q_2^I \rangle d^l_{p_1^I + p_2^I, M_1 + M_2}(\psi) \begin{pmatrix} L_1 & l & L_2 \\ M_1 & -M_2 - M_1 & M_2 \end{pmatrix} \Bigg\} R_{\mu, l}(L_1 K_1 j_1^K; L_2 K_2 j_2^K) , \tag{A56}$$

where

$$N_p(P_1^I M_1; p_2^I M_2^I) = [(1 + \delta_{p_1^I, 0}\delta_{M_1, 0})(1 + \delta_{p_2^I, 0}\delta_{M_2, 0})]^{-1/2} . \tag{A57}$$

The operator Γ_p is factored with respect to j^M in the new basis set, and its matrix elements are as before [cf. Eq. (A40)] except for the factor $\delta_{j_1^M, j_2^M}$. The starting vector $|v_p\rangle$ has components only for $j^M = 1$ and they are given in Eq. (A39). The matrix elements of L″ are

$$\langle p_1^I q_1^I; L_1 M_1 K_1 j_1^M j_1^K \,|\, \mathrm{L}''_m \,|\, p_2^I q_2^I; L_2 M_2 K_2 j_2^K \rangle = N_L(L_1, L_2) N_K(K_1, K_2) [2(1 + \delta_{M_1, 0}\delta_{p_1^I, 0})]^{-1/2} (-1)^{M_1 + K_1}$$

$$\times \sum_{\mu, l} \Bigg\{ \langle 1, 0; p_1^I, q_1^I | [A_\mu^{(l, 1 - p_1^I - p_2^I)}]^\times | 0, M; p_2^I, q_2^I \rangle d^l_{1 + p_1^I - p_2^I, M_1 - M_2}(\psi) \begin{pmatrix} L_1 & l & L_2 \\ M_1 & M_2 - M_1 & -M_2 \end{pmatrix} + j_1^M (-1)^{L_1 + M_1}$$

$$\times \langle 1, 0; -p_1^I, q_1^I | [A_\mu^{(l, 1 - p_1^I - p_2^I)}]^\times | 0, M; p_2^I, q_2^I \rangle d^l_{1 - p_1^I - p_2^I, -M_1 - M_2}(\psi) \begin{pmatrix} L_1 & l & L_2 \\ -M_1 & M_2 + M_1 & -M_2 \end{pmatrix} \Bigg\} R_{\mu, l}(L_1 K_1 j_1^K; L_2 K_2 j_2^K) , \tag{A58}$$

where the basis elements for $p_2^S = 0$ have not been changed. Note that if the perturbation contributions are not considered, the matrix $\Gamma_p - iL_p$ is factored with respect the index j^M and one needs to consider only the submatrix defined for $j_1^M - j_2^M = 1$.

APPENDIX B: MATRIX ELEMENTS OF $[A_\mu^{(l,m)}]^\times$

Let us first consider the hyperfine interaction $\mathbf{I} \cdot \mathbf{A} \cdot \mathbf{S}$. The spherical components for the vectorial operators I and S are given in terms of the equation[3,4]

$$\mathrm{A}_A(l, m) = \sum_{m_1, m_2} C(1, 1, l; m_1, m)\, \mathrm{T}_S^{(1, m_1)}\, \mathrm{T}_I^{(1, m_2)} , \tag{B1}$$

where the first rank spherical components $\mathrm{T}_I^{(1,m)}$ are defined as following:

$$\mathrm{T}_I^{(1,0)} = \mathrm{I}_z ,$$
$$\mathrm{T}_I^{(1,\pm 1)} = \mp \frac{1}{\sqrt{2}} \mathrm{I}_\pm , \tag{B2}$$

and the $C(1, 1, l; m_1, m)$ are the Clebsch–Gordan coefficients. The matrix elements of $\mathrm{T}_I^{(1,m)}$ can be written as

$$\langle m_1^I | \mathrm{T}_I^{(1,m)} | m_2^I \rangle = \delta_{m_1^I, m + m_2^I} \{ m_1^I \delta_{m,0} - m\delta_{|m|,1} \times [\mathrm{I}(I+1) - m_1^I m_2^I]^{1/2}/\sqrt{2} \} . \tag{B3}$$

It is useful also to calculate the following matrix elements for the definition of the p and q indices:

$$\langle p_1^I, q_1^I | \mathrm{T}_I^{(1,m)} \otimes 1 | p_2^I, q_2^I \rangle \equiv \delta_{(q_1^I - p_1^I)/2, (q_2^I - p_2^I)/2} \left\langle \frac{q_1^I + p_1^I}{2} \,|\, \mathrm{T}_I^{(1,m)} \,|\, \frac{q_2^I + p_2^I}{2} \right\rangle$$
$$= \delta_{\Delta p^I, \Delta q^I}\delta_{\Delta p^I, m}[\delta_{\Delta p^I, 0}(q_1^I + p_1^I)/2 - \delta_{|\Delta p^I|, 1}\Delta p^I K_I/\sqrt{2}] , \tag{B4a}$$

$$\langle p_1^I, q_1^I | 1 \otimes [\mathrm{T}_I^{(1,m)}]^{\mathrm{Tr}} | p_2^I, q_2^I \rangle \equiv \delta_{(q_1^I + p_1^I)/2, (q_2^I + p_2^I)/2} \left\langle \frac{q_1^I - p_1^I}{2} \,|\, \mathrm{T}_I^{(1,m)} \,|\, \frac{q_2^I - p_2^I}{2} \right\rangle$$
$$= \delta_{-\Delta p^I, \Delta q^I}\delta_{\Delta p^I, m}(\delta_{\Delta p^I, 0}\frac{q_1^I - p_1^I}{2} - \delta_{|\Delta p^I|, 1}\Delta p^I K_I/\sqrt{2}) , \tag{B4b}$$

where

$$\Delta p^I = p_1^I - p_2^I ,$$
$$\Delta q^I = q_1^I - q_2^I ,$$
$$K_I = [I(I+1) - (q_1^I \Delta q^I + p_1^I \Delta p^I)(q_1^I \Delta q^I + p_1^I \Delta p^I - 2)/4]^{1/2} .$$

The symbol $\otimes$ stands for the tensor (or Kronecker) product between two matrices, i.e.,

$$\langle k_1', k_1'' | \mathrm{A} \otimes \mathrm{B} | k_2', k_2'' \rangle \equiv \langle k_1' | \mathrm{A} | k_2' \rangle \langle k_1'' | \mathrm{B} | k_2'' \rangle . \tag{B5}$$

Note that the Liouville operator $A^\times$ associated with the operator A can be written as

$$\mathrm{A}^\times = \mathrm{A} \otimes 1 - 1 \otimes \mathrm{A}^{\mathrm{Tr}} . \tag{B6}$$

Analogous equations are derived for the electron spin operator. We can now calculate from Eq. (B1), the matrix elements of $[A_A^{(l,m)}]^\times$:

$$\langle p_1^S, q_1^S; p_1^I, q_1^I | [A_A^{(l,m)}]^\times | p_2^S, q_2^S; p_2^I, q_2^I \rangle = \delta_{m, \Delta p}\delta_{|\Delta p^S|, |\Delta q^S|}\delta_{|\Delta p^I|, |\Delta q^I|} \times \delta_{\Delta p^S, \Delta p^I}\delta_{\Delta q^S, \Delta q^I} C(1, 1, L; \Delta p^S, \Delta p^I, \Delta p) S_A , \tag{B7}$$

where $\Delta p \equiv \Delta p^S + \Delta p^I$ and the quantity S_A assumes these possible values:

$$\Delta p^S = 0, \quad \Delta p^I = 0, \quad S_A = (p_1^S q_1^I + p_1^I q_1^S)/2 ,$$

$$\Delta p^S = 0, \quad \Delta p^I = 0, \quad S_A = -(p_1^S \Delta p^I + q_1^S \Delta q^I) K_I/\sqrt{8} ,$$

$$\Delta p^S \neq 0, \quad \Delta p^I = 0, \quad S_A = -(p_1^I \Delta p^S + q_1^I \Delta q^S)/\sqrt{8} ,$$

$$\Delta p^S \neq 0, \quad \Delta p^I = 0, \quad S_A = \Delta p^S \Delta q^I K_I/2 .$$

The matrix elements for $[A_g^{(l,m)}]^x$ are derived with the same procedure:

$$\langle p_1, q_1; p_1^I, q_1^I | [A_g^{(l,m)}]^x | p_2, q_2; p_2^I q_2^I \rangle = \delta_{\Delta p^I,0} \delta_{\Delta q^I,0} \delta_{|\Delta p|,|\Delta g|} \delta_{\Delta p,m} B_0 C(1, 1, l; \Delta p, 0, \Delta p) S_g , \quad \text{(B8)}$$

where S_g is defined as

$$\Delta p^S = 0, \quad S_g = p_1^S B_0 ,$$

$$\Delta p^S \neq 0, \quad S_g = -\Delta q^S B_0/\sqrt{2} .$$

These matrix elements have the following symmetry property:

$$\langle -p_1^S, q_1^S; -p_1^I, q_1^I | [A_\mu^{(l,-m)}]^x | -p_2^S, q_2^S; -p_2^I, q_2^I \rangle = (-1)^{1+\Delta p^S + \Delta p^I} \langle p_1^S, q_1^S; p_1^I, q_1^I | [A_\mu^{(l,m)}]^x | p_2^S, q_2^S; p_2^I, q_2^I \rangle . \quad \text{(B9)}$$

[1](a) C. F. Polnaszek and J. H. Freed, J. Phys. Chem. 79, 2283 (1975); (b) W. J. Lin and J. H. Freed, *ibid.* 83, 379 (1979).

[2](a) K. V. S. Rao, C. F. Polnaszek, and J. H. Freed, J. Phys. Chem. 81, 449 (1977); (b) C. F. Polnaszek, G. V. Bruno, and J. H. Freed, J. Chem. Phys. 58, 3185 (1973); (c) J. H. Freed, *ibid.* 66, 4183 (1977).

[3](a) E. Meirovitch and J. H. Freed, J. Phys. Chem. 84, 2459 (1980); (b) 84, 3281 (1980); (c) 84, 3295 (1980); (d) More recent work, however, [L. Kar, E. Igner, and J. H. Freed (unpublished)] has indicated that the matter may be more complex and may involve precise details of the preparation and annealing of the multibilayers of this lyotropic material .

[4](a) G. R. Luckhurst and M. Setaka, Mol. Cryst. Liq. Cryst. 19, 179 (1972); (b) G. R. Luckhurst, M. Setaka, and C. Zannoni, Mol. Phys. 28, 49 (1974).

[5](a) F. Pusnick, M. Schara, and M. Sentjurc, J. Phys. (Paris) 36, 665 (1975); (b) F. Pusnick and M. Schara, Chem. Phys. Lett. 37, 106 (1976).

[6](a) G. R. Luckhurst and A. Sanson, Mol. Phys. 24, 1297 (1972); (b) G. R. Luckhurst, M. Ptak, and A. Sanson, J. Chem. Soc. Faraday Trans. 2 69, 1752 (1973); (c) D. Sy and and M. Ptak, Mol. Cryst. Liq. Cryst. 39, 53 (1977); (d) M. A. Hemminga, J. Magn. Reson. 25, 25 (1977).

[7]G. R. Luckhurst *et al.*, J. Magn. Reson. 42, 351 (1981).

[8]A. E. Stillman and J. H. Freed, J. Chem. Phys. 72, 550 (1980).

[9]L. P. Hwang and Freed, J. Chem. Phys. 63, 118 (1975).

[10](a) F. Barbarin, D. Cabaret, B. Chevarin, C. Fabre, and J. P. Germain, Mol. Cryst. Liq. Cryst. 46, 181, 195 (1978); (b) F. Barbarin, B. Chevarin, and J. Germain, J. Phys. 40, C3, 153 (1979); (c) F. Barbarin, J. P. Chausse, C. Fabre, and J. P. Germain, *ibid.* 42, 1183 (1981). Barbarin *et al.* used the longer $C_8H_{17}O$ chain in (a) and (b) and the shorter chain C_2H_5O in (c) compared to our use of C_4H_9O, cf. Fig. 1. In the recent work of part (c) these authors study the motional dynamics of their C_2H_4O probe in 40, 8 but use a simple motional narrowing approach with a "strong-collision" model without the benefit of angular-dependent line-shape measurements, so it is not surprising there are differences in details of analysis vs our study of P in 40, 6, which employs a full line shape (and slow-motional) analysis and a Brownian motion model.

[11]Good summaries of the properties of these types of liquid crystals may be found in *The Molecular Physics of Liquid Crystals*, edited by G. R. Luckhurst and G. W. Gray (Academic, New York, 1979); Chap. 12 by G. W. Gray, Chap. 13 by A. J. Leadbetter, Chap. 14 by J. Doucet.

[12](a) G. Moro, TRIDG (unpublished report, Cornell University, 1980); (b) G. Moro and J. H. Freed, J. Phys. Chem. 84, 2837 (1980); (c) J. Chem. Phys. 74, 3757 (1981).

[13](a) Flexible deuterated probes somewhat related to P have been used previously to study side-chain motion in polymers [cf. J. Pilar, J. Labsky, J. Kalal, and J. H. Freed, J. Phys. Chem. 83, 1907 (1979)]. Rotation about the piperidine x''' axis was typically four to six times faster than about the other axes, and τ_R decreases with chain length to the asymptotic value of the free piperidine, but in all cases the $E_a \approx 3.6$ kcal/mol; (b) G. R. Luckhurst and R. Poupko, Mol. Phys. 29, 1293 (1975), and references therein.

[14](a) J. A. Murphy, Mol. Cryst. Liq. Cryst. 22, 133 (1973); (b) P. G. deGennes, *The Physics of Liquid Crystals* (Oxford, New York, 1974); (c) S. A. Pikin, Mol. Cryst. Liq. Cryst. 63, 181 (1981); (d) Very small regions near each glass surface, of $\sim 2\,\mu$ thickness out of a sample thickness of 200 μ did exhibit some misalignment under the microscope, but this was judged to be an insignificant fraction of the sample, so no effort was made to ensure perpendicular alignment on the plate surfaces.

[15](a) J. S. Hwang, R. P. Mason, L. P. Hwang, and J. H. Freed, J. Phys. Chem. 79, 489 (1975); (b) J. H. Freed, J. Chem. Phys. 41, 2077 (1964).

[16]The definition of λ here is a little different than that used by Polnaszek and Freed [Ref. 1(a)]. Thus, $\lambda = (2/3), \lambda^{PF}$. Also $\rho = (2/\sqrt{6})\,\rho^{PF}$.

[17]A. de Vries, Mol. Cryst. Liq. Cryst. 63, 215 (1981), and references therein.

[18](a) P. A. C. Gane, A. J. Leadbetter, and P. G. Wrighton, Mol. Cryst. Liq. Cryst. 66, 247 (1981); (b) P. S. Pershan, G. Aeppli, J. A. Litster, and R. J. Birgeneau *ibid.* 67, 205 (1981).

[19]Somewhat different behavior has been observed for the large and *rigid* probe CSL in 40, 6 [cf. Ref. 3(a)]. It exhibits values of $\tau_{R_\perp}$ that are approximately an order of magnitude longer than for P, as well as significantly larger ordering. Large SRLS effects were postulated in both the S_A and S_B phases for CSL, but the low resolution of the ESR spectra and the lack of an orientation-dependent study does somewhat reduce the reliability of those studies. Nevertheless, the inferred existence of a SRLS mechanism for CSL does correlate well with the strong cooperativity for reorientation expected especially in the S_B phase.

[20](a) E. Meirovitch (unpublished results); (b) On the other hand, if PDT were located in the chain region and the cooperative chain distortion mode exists, then rapid enough translational diffusion of PDT could average out such inhomogeneities, but it could not be expected to average out inhomogeneities in macroscopic alignment.

[21](a) This comes about in the following way. The range of y_l^c values between y_l^c and $y_l^c + \delta y_l^c$ which correspond to a particular value of $n_{l,g}^c$ is

$$P(\theta') \propto \delta y_l^c = \delta(\cos\theta') \left[\frac{dn_{l,g}^c}{dy_l^c}\right]^{-1} \propto 1/\sin\theta' .$$

(b) More generally, we can have a distribution in values of pitch p (corresponding, e.g., to a Fourier decomposition of the chain distortions). Only those Fourier components with p satisfying this inequality would contribute to the static distribution function $P(\theta', \phi')$. (c) We have in recent work found that line shapes quite similar to those obtained with the $(\sin\theta')^{-1}$ distribution could be obtained with a small admixture

(~20%) of a well aligned spectrum with a nearly random distribution (~80%). Such a large misalignment is ruled out by our optical observations under a polarizing microscope (Sec. II) and by the well-aligned results with CSL [cf. Fig. 5(c)] and PDT.

[22](a) The calculated series of line shapes corresponding to the experimental spectra recorded at −9 °C involved storage requirements which were limiting for the PDP-11 minicomputer. Since these spectra might be slightly nonconverging we assign a larger error to the −9 °C point in Fig. 2. (b) Actually, it is possible that as the temperature is lowered the bilayer structure becomes more like a monolayer, cf. G. J. Brownsey and A. J. Leadbetter, Phys. Rev. Lett. **44**, 1608 (1980), who have found *two* mass density fluctuations of incommensurate wavelength.

[23](a) One could conceive of the possiblity that different probes exhibit different "solubility" in regions of different alignment. That is, CSL might preferentially seek out well-aligned regions, while P probe might prefer more disordered regions of the sample. Our observations under the polarizing microscope are, of course, inconsistent with the existence of such regions except if they were submicroscopic in size (and/or relaxing too fast to be seen optically, but slow on ESR time values). One would then require periodic distortion modes in the disordered regions, that need not necessarily involve just the alkyl chains in order to "explain" our P probe ESR results. The pitch of such a mode must be large enough that the P probe diffusion (and/or relaxation of the mode or its propagation relative to the probe location) cannot average out the spectral effects of the distortion mode. This domainlike model seems to us less consistent with the known properties of liquid crystals than the model used in the main text, although the possibility of submicroscopic regions of faults or dislocations into which some probes may segregate could be of importance, but it is likely to lead to exchange narrowing effects on the ESR spectrum. *Note added proof*: A. M. Levelut and C. Druon, [J. Phys. Lett. **43**, 193 (1982)] have recently suggested, from x-ray and dielectric measurements on another cyanobiphenyl, the existence of tilted monolayer cybotactic groups of molecules inside a partially bilayer smectic *A* phase, with all linear dimensions of such groups corresponding approximately to eight molecular lengths and with a tilt angle of about 35°, Since the cybotactic clusters are found only at lower temperature, the possibility exists that *P* probe is preferentially soluble in such clusters. For such small clusters of the size reported, any inhomogeneities in the ordering of the molecules should be averaged out in the ESR by translational diffusion within such a cluster. Thus, one might consider the possibility of, e.g., different degrees of chain tilt (cf. Fig. 7) for the different cybotactic clusters, which is then sensed by the *P* probe. The CSL, on the other hand, could be almost entirely in the normal smectic *A* bilayers. (b) S. A. Goldman, G. V. Bruno, C. F. Polnaszek, and J. H. Freed, J. Chem. Phys. **56**, 716 (1972).

[24]A. J. Leadbetter, J. C. Frost, J. P. Gaughan, G. W. Gray, and A. Mosley, J. Phys. Paris 40, 375 (1979).

[25](a) P. G. de Gennes, Solid State Commun. 6, 163 (1968); G. R. Luckhurst and H. J. Smith, Mol. Cryst. Liq. Cryst. 20, 319 (1973). (b) Another possiblity would be to restrict $P(\theta', \phi')$ to be zero for values of θ' greater than some value $\theta'_{max} < 90°$. We found from our simulations that for θ'_{max} significantly less than 90° (e.g., 75°–80°), poorer agreement with experiment was found. (c) An even more dramatic discrepancy of this general character was noted in Ref. 3(c) in the study of the stearamide probe in the $L_\alpha(1)$ lipid phase. While in tube samples an $a_N = 16.2$ G was found, oriented plate samples yielded an apparent $a_N = 19.05$ G. It was suggested in that work [Ref. 3(c)] that (1) the well-aligned plate samples had large arrays of uniform bilayers with strong cooperative interbilayer forces prevailing in the headgroup regions (and this was not so for tube samples) and (2) the stearamide could take on an ordered conformation similar to the lipid molecules with its chain aligned with the lipid chains and its piperidine ring aligned *perpendicular* to the chains and located in the fluid head-group region. It was further postulated that the piperidine ring would be substantially ordered to exhibit an apparent $a_N = 19.05$ G even though one usually expects this piperidine ring to be weakly ordered due to its extensive flexibility. If instead, we merely assume that the 90° twist of the piperidine ring significnatly *increases* a_N by analogy to our above discussion of P probe, then it would no longer by necessary to invoke appreciable ordering of this probe to explain this unusual experimental result.

[26]G. Moro, Implementation of the Lanczos Algorithm in the Calculation of Spectral Functions (unpublished report, Cornell University, 1980).

[27]M. E. Rose, *Elementary Theory of Angular Momentum* (Wiley, New York, 1957).

[28]P. L. Nordio, in *Spin Labelling: Theory and Applications*, edited by L. J. Berliner (Academic, New York, 1976) uses these conventions.

[29]J. H. Freed, in *Spin Labeling: Theory and Applications*, edited by L. J. Berliner (Academic, New York, 1976). Here the Freed–Franekel conventions [J. Chem. Phys. 39, 326 (1963)] are used.

[30]R. F. Campbell, E. Meirovitch, and J. H. Freed, J. Phys. Chem. 83, 525 (1979).

[31]S. Alexander, A. Baram, and Z. Luz, Mol. Phys. 27, 441 (1974).

[32]M. P. Eastman, R. G. Kooser, M. R. Das, and J. H. Freed, J. Chem. Phys. 51, 2690 (1969); J. H. Freed, J. Phys. Chem. 71, 38 (1967).

[33](a) More generally, one must replace S_x by the magnetization $M_x \approx \sum_i g_{xi} S_i$, but this is only important for a very anisotropic g tensor [cf. R. F. Campbell and J. H. Freed, J. Phys. Chem. **84**, 2668 (1980)]; (b) An earlier version is given by Campbell and Freed (*ibid.*).

[34]E. C. Kemble, *The Fundamental Principles of Quantum Mechanics with Elementary Applications* (Dover, New York, 1958), p. 394.